Aleksej Samojlov, BSc.

On the preparation of macroporous polydivinylbenzene nanocomposite foams and their carbonisation

MASTER'S THESIS

To achieve the university degree of

Diplom-Ingenieur

Master's degree programme: Technical Chemistry

submitted to

Graz University of Technology

Supervisor

Univ.-Doz. Dipl. Ing. Dr. techn. Christian Slugovc

Institute for Chemistry and Technology of Materials

2015

Acknowledgements

First of all I would like to thank my advisor Prof. Christian Slugovc for giving me the opportunity to work on this interesting topic, and for the great supervision. Thank you for your advice and for sowing the seeds of new ideas.

I am grateful to Dr. Stefan Freunberger for introducing the topic of lithium-air batteries to our university.

Many thanks to Prof. Gregor Trimmel and his employees Verena Kaltenhauser and Christine Buchmaier for help with the topic of xanthates, as well as Sebastijan Kovačič for advice on polyHIPE preparation and analysis.

Some important tasks had to be outsourced to Josefine Hobisch who did thermal analysis, Johann Schlegl who helped with lathing the samples, Franz-Andreas Mautner and Brigitte Bitschnau who recorded X-ray diffraction spectres, and Katharina Gruber who carbonised a few samples, for which I am very grateful.

Special thanks go to Bettina Grumm, Simone Strasser and Christina Wappl who made me take microbreaks every now and then, thus enhancing my productivity, and also for all the inspiring discussions on my research topic. Furthermore, I would also like to thank all members of the Institute for Chemistry and Technology of Materials for providing a productive and friendly atmosphere at work.

I would also like to show my gratitude to my beloved girlfriend who made me take my mind off all the science-stuff and enjoy her delicious food and some tea in a cosy, homely environment.

Last but not least, I owe my deepest gratitude to my family who made it possible for me to make it all the way through my course of studies, and create this scientific work. Thank you for supporting and motivating me in any ways possible, and especially for all the times when you pointed me in the right direction.

AFFIDAVIT

I declare that I have authored this thesis independently, that I have not used other than the declared sources/resources, and that I have explicitly indicated all material which has been quoted either literally or by content from the sources used. The text document uploaded to TUGRAZonline is identical to the present master's thesis.

EIDESSTATTLICHE ERKLÄRUNG

Ich erkläre an Eides statt, dass ich die vorliegende Arbeit selbstständig verfasst, andere als die angegebenen Quellen/Hilfsmittel nicht benutzt, und die den benutzten Quellen wörtlich und inhaltlich entnommenen Stellen als solche kenntlich gemacht habe. Das in TUGRAZonline hochgeladene Textdokument ist mit der vorliegenden Diplomarbeit identisch.

_____   _____
          Datum   Unterschrift

Abstract

Polymerised high internal phase emulsions (pHIPEs) can be found in a variety of fields and compositions. Amongst other things, they can be used as templating materials for porous carbons, which in turn have a plethora of applications of their own. This work deals with the formulation of carbon foams with incorporated moieties of metal sulphides or carbides, which are seen as possible cathode materials for future designs of lithium-air batteries.

In the primary step, metal xanthates (metal dithiocarbonates) were ingested into the continuous phases of surfactant stabilised water-in-monomer high internal phase emulsions. During subsequent polymerisation of the continuous phase, the metal-xanthates were entrapped inside the polymer and were subsequently transformed into the corresponding metal-sulphides through heat treatment. The resulting macroporous nanocomposite polymer foams were carbonised afterwards, resulting in highly interconnected carbonaceous foams with nanometer-scaled metal sulphide moieties.

Several of these foams were produced, whereby the stages of production were investigated by SEM, EDX and XRD.

Kurzfassung

Von der Herstellung makroporöser Polydivinylbenzen-Nanokompositschäume und ihrer Karbonisation

Polymerised High Internal Phase Emulsions (pHIPEs) sind in einer Vielzahl von Arten und Zusammensetzungen zu finden. Unter anderem werden sie als Schablonenmaterial für porösen Kohlenstoff verwendet, welcher wiederum selbst zahlreiche Anwendungsmöglichkeiten besitzt. Die vorliegende Arbeit beschreibt die Erstellung von Kohlenstoffschäumen mit eingebundenen Sulfid- oder Carbidanteilen, welche als mögliche Kathodenmaterialien für zukünftige Bauarten von Lithium-Luft Batterien angesehen werden.

Im ersten Schritt wurden Metallxanthate (Metalldithiocarbonate) in die kontinuierliche Phase von einer mit einem Tensid stabilisierten Wasser-in-Monomer High Internal Phase Emulsion aufgenommen. Während der nachfolgenden Polymerisation der kontinuierlichen Phase wurden die Metallxanthate im Polymer eingeschlossen, und anschließend durch Wärmebehandlung in die entsprechenden Metallsulfide umgewandelt. Die resultierenden makroporösen Nanoverbundpolymerschäume wurden karbonisiert, wobei durchgehend poröse Kohlenstoffschäume mit nanometergroßen Metallsulfideinschlüssen erzeugt wurden.

Es wurden mehrere dieser Schäume hergestellt, wobei die einzelnen Herstellungsstadien durch SEM, EDX und XRD kontrolliert wurden.

Table of Contents

1. Introduction

During mankinds perpetual struggle for resources, especially for energy carriers, it became more and more common to aspire for diversity of raw materials, as well as using substances that are abundant in all regions of the world.

As fossil fuels are slowly becoming harder to come by and thus are getting more expensive, mankind seeks for more diversity in means of generation and storage of energy to maintain the habitual levels of comfort, particularly in means of personal transportation. Since energy density of a storage system is a major concern for mobility applications in general, purely electrical vehicles were at a major disadvantage: The energy used to power the engines had either to be supplied to the vehicle, or to be carried along in the form of a battery. The former allows a lightweight construction of the vehicle but strongly limits the flexibility of possible routes, since such a vehicle is confined by the range of a cable or a route of rails, which precludes the possibility of even minor manoeuvring. Vehicles with built-in batteries provide an elevated degree of flexibility, but still have to carry the weight of the energy storage device at all times.

Earlier designs of batteries were large and heavy (~60 Wh kg^{-1} for lead-acid batteries), in scientific terms: they had low energy densities. This was a result of both the relatively crude state of technology as well as the highest achievable energy densities of the utilised electrochemical reactions. Since then, major leaps were made elaborating existing systems and implementing the ones that were formerly unused. Though in the present days rechargeable lithium-ion batteries are standard in almost all portable consumer electronics and even in electric vehicles, their comparably lower energy density (~245 Wh kg^{-1}) as well as other issues still prevent it from being a real competitor for internal combustion engines (~700 Wh kg^{-1}) in the field of personal transport.[1]

Of these newer designs one shall be the focused on in the present work. Standing out before its competitive systems is the aprotic lithium-air battery. With a calculated specific mass energy density of 3458 Wh kg^{-1} one could assume an even better energy density than with use of internal combustion engines. However, Table 1 illustrates a series of widely used rechargeable battery systems and shows that calculated values are never achieved even in well developed systems such as the nickel-cadmium or lead-acid batteries.

**Table 1: Specific energy densities for various battery systems[1]**

| System	Mass-specific energy density (Wh kg^{-1})			Volume-specific energy density (Wh L^{-1})	
	Calculated	Practical	Conversion yield[a]	Calculated	Practical
Li/O$_2$	3458	?		6170	?
Li/S	2566	350[b]	0.128	4260	350[b]
Zn/air	1086	180[c]	0.166	6091	208[c]
C/LiCoO$_2$	387	100[d] 245[e]	0.258 0.633	1015	150[d] 585[e]
M-H/NiOOH	180	63[f] 58[g]	0.35 0.32		142[f] 84[g]
Pb/PbO	171	60,6	0.35	370	108[g]
[a]Practical/calculated energy density, [b]ca. 5 Wh, [c]120 Wh, [d]375 Wh, [e]12 Wh, [f]1.14 Wh, [g]336 Wh					

Following the development of these battery systems, one could speculate on an implementation degree of lithium-air batteries ranging from 14 to 35% of the calculated values, hence providing a rechargeable battery with an energy density of approximately 120 to 480 Wh kg^{-1}. Such values could promote the lithium-air battery as a competitor for vehicles with internal combustion engines.

1.1.   Lithium-air battery

The Li-air battery system was introduced by Abraham and Jang in 1996[2] however, interest in this system was rather low for the time of the following decade. There are two concepts for Li-air battery systems: aqueous and nonaqueous[3] (or aprotic). The fundamental cell reaction of the former type is the formation of lithium peroxide from oxygen of the atmosphere and lithium as follows

$$2\,\mathrm{Li} \;+\; \mathrm{O_2} \rightarrow \mathrm{Li_2O_2}$$
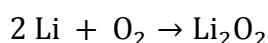
The aqueous concept involves water molecules in the reaction as well.

$$4\,\mathrm{Li} + 6\,\mathrm{H_2O} + \mathrm{O_2} \rightarrow 4\,(\mathrm{LiOH \cdot H_2O})$$
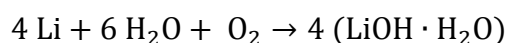
Although both exhibit high energy densities on paper, the aqueous concept suffers from LiOH solubility issues in practice, making the aprotic approach more promising. Working prototypes of aprotic batteries have already been built,[4,5] but the system still has drawbacks of its own. One major drawback at the time is poor electrolyte stability. In the course of charging and discharging, the electrolyte slowly decomposes, drastically reducing cycle stability and therefore also capacity and

lifetime of the battery. It has been shown that an implementation of proper cathode materials as TiC in place of carbon prevents electrolyte decomposition, greatly improving cycle stability.[6] However, this material has yet to be brought into a shape that could harness the vast possibilities of this electrochemical system.

Li_2O_2 which is produced during the discharge process has poor electron conducting properties, making it necessary to store it in very small portions that have to be electrically contacted by the cathode material. In order to distribute these throughout the cathode, it has to possess a highly porous structure with small sized pores. Furthermore, it has to allow oxygen diffusion to every pore, making an interconnected structure crucial. Considering all these requirements, it seems that polyHIPEs made from or coated with TiC would make for a good cathode material.

1.2.　　polyHIPEs

Porous polymers are often part of our everyday life: often used as packaging materials or insulators against heat or noise, many of their kind are surrounding us from day to day. However, this is but a small fraction of the possible applications of porous polymers which include but are not limited to the use as separation membranes, biomedical devices, high-performance microelectronics, polymer-supported reagents and catalysts, templates for porous inorganics and more.[7] There are also several means for the production of porous polymers with an even wider variety of utilised polymers, many of which generate materials with outstanding chemical and mechanical properties, but closed cells. However, since an open-cellular structure is vital for the future use of the material to be produced, one rather sophisticated method prevails.

Polymer foams templated by means of high internal phase emulsions (polyHIPE) possess a structure of interconnected voids which makes their structure ideal for the task at hand.

1.3.　　Xanthates

Xanthates derive from the xanthic acid whereby the term xanthates is used both for the O,S-diesters as well as the metal salts whereby the latter are of interest to the present work. All three are depicted in Figure 1. Xanthates can be seen as relatives of esters of carbonic acid, where two oxygen atoms are replaced by sulphur, thus the

IUPAC name dithiocarbonates and accordingly O-alkyldithiocarbonates[8,9] which will be discussed on the following pages.
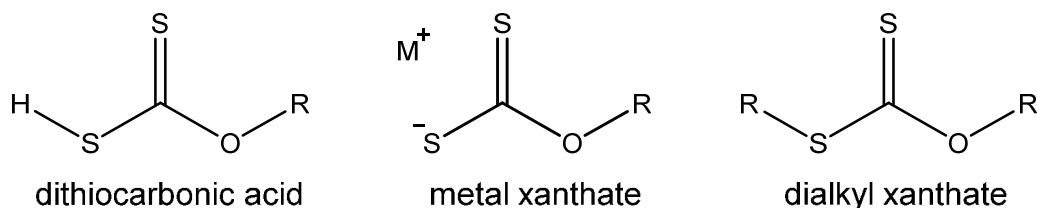

Figure 1: Dithiocarbonic acid and related compounds

The name xanthogenates is derived from the Greek ξανθός [ksant^{h}ós], which translates as: "yellowish, golden" and was introduced by Zeise, who discovered this class of compounds as early as 1822.[10] Since that time, they became more often referred to as xanthates, and with time many uses were discovered for this class of compounds. To name only a few, xanthates are important intermediates in the production of cellulose fibers and cellophane. Because of their convenient properties as a detergent they are widely used as flotation agents in the refinement process of mineral ores. In rubber production they can be used as antioxidants and as vulcanisation accelerators. Further, they are used in pharmaceutics, environmental chemistry, agriculture, polymer production, analytics of heavy metals and many more.[8]

From this plethora of applications, only one is used in this work: the thermal decomposition via the Chugaev-reaction.[11] When heated until decomposition temperature, Xanthates decompose into the according metal sulphides, liberating a variety of mostly gaseous substances.[12,13]

2. Aim of this work

As described by Thotiyl[14] there is a way of constructing a working Li-air battery with a good cycle stability by using a cathode made of TiC, since this material does not enter side reactions with the electrolyte to form unwanted carbonate-byproducts. Unfortunately this material is not easily formed into an arbitrary shape due to its exceptional hardness (microhardness of ~3000 kg mm^{-2} [15] Mohs hardness of 8-9 [16]) so that it appears necessary to fit it as required as soon as during production. One possible option for the preparation of carbides is the reaction of the according metal or metal oxide with carbon or graphite at temperatures reaching from 1000 to 1500 °C.[15]

With some adjustments, the mentioned system should as well be applicable with the corresponding metal sulphides and a carbonised polymer. Since metal sulphides can be prepared with relative ease from metal xanthates, it appears possible to prepare a solution of xanthate in a monomer and polymerise it into a polyHIPE, thus creating a foam with xanthate molecules entrapped within the polymer chains. The xanthates can be converted into sulphides during a subsequent tempering step and should create finely distributed sulphide moieties inside the bulk parts of the foam. After this tempering step, the polymer has to be carbonised in order to obtain a porous, carbonaceous matrix with embedded sulphide moieties, which in turn has to be heated to carbonisation temperatures in order to produce carbides.

Through all these aforementioned steps, which are additionally illustrated in Figure 2, the interconnected morphology of the pHIPEs should be retained, providing highly porous metal carbide composite foams with an ample surface area and conductivity and also enough mechanical stability to be integrated into Li-air batteries.
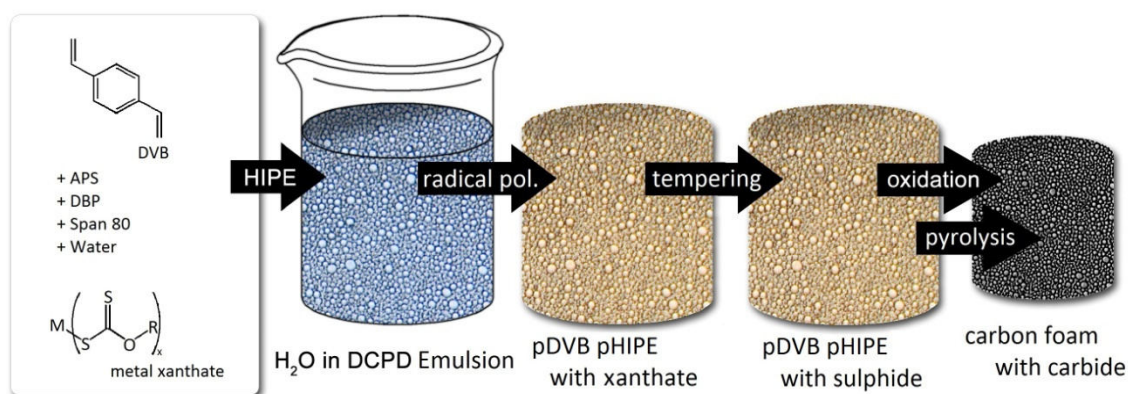
Figure 2: Workflow and goal[17]

Since types of metal xanthates are manifold, but posses certain similar properties as a group of compounds, a model system shall be developed on the basis of a selected few. The model system should provide the possibility to assess if incorporation of metal can be conducted to a sufficient degree trough in-situ polymerisation of xanthate solutions, and if this route of production is promising in general. If not, it should provide a base for other pathways towards said composite materials.

3. Technologies – State of the art

3.1.   Preparation of xanthates

A basic means of preparation is the reaction of an alcohol, carbon disulfide and an alkali hydroxyl with elimination of water and is illustrated in Figure 3.

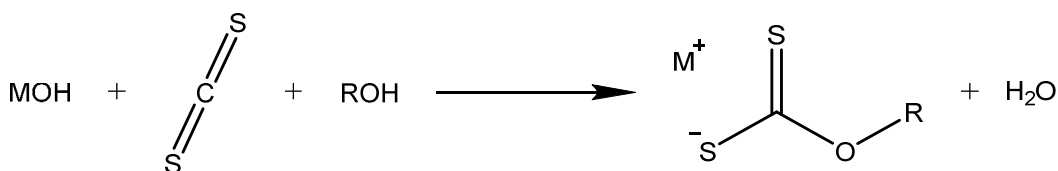**Figure 3: Preparation of metal xanthates**

Although it is a one pot reaction, Gomez showed that it is actually two bimolecular reactions occurring consecutively[9,18] (Figure 4)
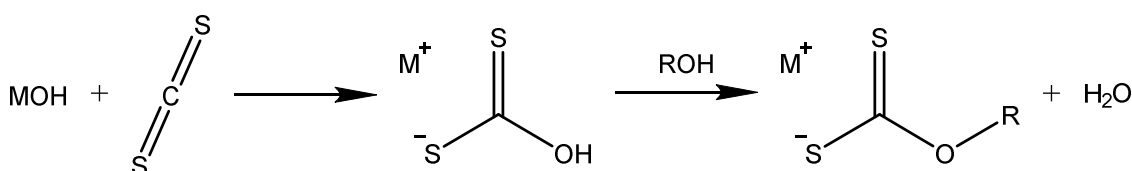
Figure 4: Bimolecular reactions leading to xanthates

Unfortunately, carbon disulphide tends to form oligo- and polysulphides in alkaline solution. In some cases these are hard to separate from the intended product due to the similar solubility.

Another route towards alkali metal xanthates lies in using t-BuOK an alcohol and carbon disulfide in a dry atmosphere.[19,20] This synthesis pathway suppresses the formation of oligo- and polysulphides and leads to high purity products but requires slightly more effort since water has to be excluded.
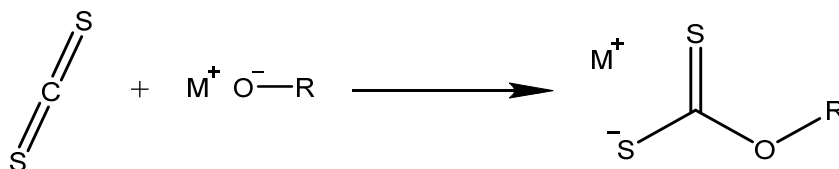
Figure 5: Alkoxide route towards metal xanthates

For many purposes, xanthates of other metals than sodium or potassium are required. Since the routes described above usually yield sodium or potassium xanthates, a transmetallation reaction is necessary to introduce transition metals into the product. The reaction shown in Figure 6 illustrates an alkali metal xanthate reacting with a metal chloride of the desired metal, where M^1 is usually sodium or potassium and M^2 can be any transition metal, and x equals the oxidation state of the

7

metal. Since the generated potassium or sodium chlorides have a good solubility in water and are furthermore very stable compounds, the transmetallation reaction is provided with enough driving force to proceed without side reactions and at moderate conditions. Another convenient side effect are the different polarity values of the two products: since the present work covers mainly xanthates with rather large, unpolar residues, separation of these from the generated salts is a piece of cake.
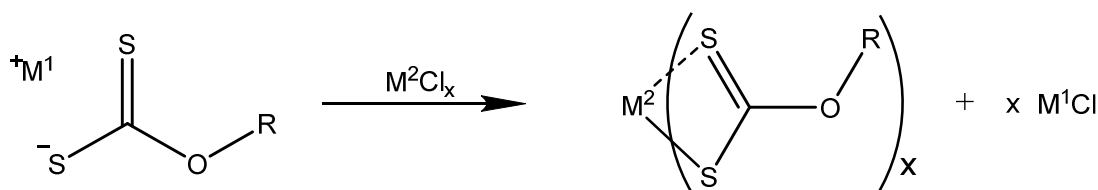
Figure 6: Transmetallation of xanthates

3.2.   Xanthates as Precursors

The research groups of Efrima[21,22] and O'Brien[23–27] showed that xanthates are versatile precursors for the synthesis of metal sulphides, both in terms of variability of the metal, as well as the alkyl side chains. Fischereder[28] showed one possible application of an in-situ formation of metal sulphide nanoparticles inside a matrix polymer.

The final purpose of xanthates in this work is, how petty it may seem, their decomposition. Under inert conditions metal xanthates decompose through a Chugaev type reaction[13] forming metal sulphides, alongside of several gaseous compounds, including alkenes, alkynes dixanthogens, alcohols, dialkyl xanthates, mercaptans and mercaptides.[9,12,13] Figure 7 shows the decomposition of a metal xanthate where M stands for a generic transition metal with x xanthate residues.

Figure 7: Thermal decomposition of metal xanthates

Due to the homogenous distribution of xanthate molecules inside the polymer matrix, the resulting sulphide moieties become very small, i.e. in the range of 1-20 nanometers.[21–27]

3.3.   Porous polymers

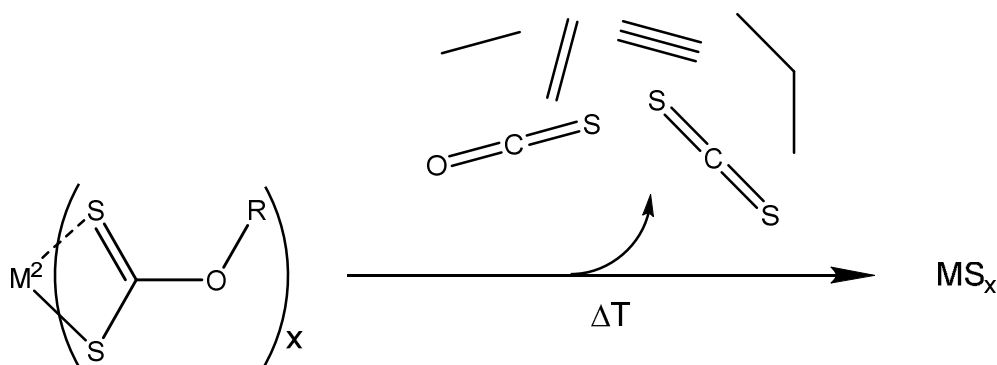Porous polymers can be categorised according to pore size. According to IUPAC, micropores are defined as pores which widths do not exceed 2 nm, while those with pore sizes of under 50 nm are called mesopores, and those which exceed this threshold are called macropores.[29] The smaller the pores of a foam, the higher its surface area. Therefore, microporous foams exhibit vast values of up to 3000 $m^2\,g^{-1}$, which can be measured by analysis of gas-adsorption isotherms through the Brunauer-Emmet-Teller model called BET.[30]

3.3.1. polyHIPEs

Emulsions are mixtures of two immiscible liquids where droplets of the internal phase are dispersed in a continuous phase. They usually are stabilised by an emulsifier, most commonly a surfactant, which composes the interface between the two phases. Hereby should be noted that whichever phase the surfactant is soluble in, will compose the continuous phase.[7,31] The maximum volume content of internal phase for monodispersed, spherical droplets is defined in the Kepler-Conjecture[32] as

$$\frac{\pi}{3\sqrt{2}} = 0.740480489 \dots$$

This equates to the hexagonal close-packing of monodispersed spheres. If the droplets are squeezed together so they lose their spherical shape, higher volume fractions of 99% of internal phase and higher are possible.

Still, a phase inversion of an emulsion remains possible above this critical level of internal phase, where an oil-in-water (o/w) emulsion will transform into a water-in-oil (w/o) emulsion and vice versa. However, this is a problem which can be dealt with by careful choice of surfactant. In this respect (on that note) it is crucial that the surfactant of the system is soluble exclusively in the continuous phase and completely insoluble in the dispersed phase of the system.[33] This property is described by a parameter named hydrophilic-lipophilic balance (HLB), which is calculated from the ratio of the mass of the lipophilic residue to the molar mass of the

9

whole molecule. The values range from 0 to 20, with 0 indicating a completely hydrophobic and lipophilic molecule.[34,35]

Furthermore, the mixture has to be mechanically agitated in order to form a HIPE. This is accomplished using a mechanical overhead stirrer since conventional magnetic stirrers do not provide enough shear force for HIPE formation and sufficient power to overcome the viscosity of the resulting HIPEs. Of course, the high internal phase ratio can also be achieved through a higher polydispersity of the
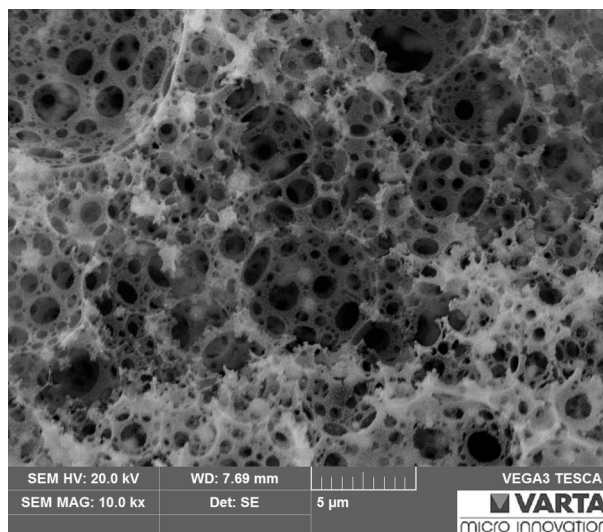
Figure 8: SEM of a polyHIPE with 95% porosity

spherical droplets, but the deformation of monodispersed spherical droplets into polyhedral droplets seems to be favourable.[36] The longer the mixture is stirred, the less polydisperse the droplets get, the more viscous it becomes, due to the increased viscosity of the system.[37] To further increase the stability of the emulsion it is recommended to add salt to the aqueous phase of W/O HIPEs. The salts reduce the solubility of nonionic surfactants and continouous phase in the aqueous phase and promote interaction between surfactant molecules, thus increasing both the elastic modulus and yield stress,[38] and furthermore reducing Ostwald ripening to a minimum.[39] Elevated temperature on the other hand, reduces HIPE stability[40–42] what in turn makes the use of temperature activated initiators more difficult.

The two phased nature of the templating system presents the choice whether to use an initiator which itself is soluble in the internal or in the external phase. The choice determines whether the polymerisation starts at the interface, as it is the case with initiators dissolved in the aqueous phase, or in the bulk, causing a more randomized polymerisation.[43]

When a HIPE is made using a suitable monomer as a continuous phase and polymerised afterwards, it is called polyHIPE as it is a polymerised High Internal Phase Emulsion as named in the first patent on this topic.[44] The internal phase can be completely removed after polymerisation through evaporation. This is made possible by the breakage of the frail thin parts of the polymer in between the droplets during curing due to shrinkage phenomena of the polymer,[33] although the surfactant

amount has to be higher than a certain amount for this to happen.[45] When these windows are formed, the voids become connected and thus a bicontinuous interconnected network is formed.[7]

Since the droplets templating the polymer foam have diameters in the range of several μm, the surface area of the resulting foams is moderate in comparison to other polymer foams. However, through the addition of a suitable porogenic solvent to the monomer phase, additional micropores are generated throughout the solid, thus raising the surface area from usual 5-20 $m^2\,g^{-1}$ in simple polyHIPEs to up to 1200 m^2/g in combination with additional treatment.[46]

Combined with the completely interconnected character of the voids, a polyHIPE exhibits a structure which is perfect for the use as a cathode in Li-O_2 batteries, although the material itself remains an issue – especially the conductivity.

3.3.2. Porous carbon

It is possible to produce a conducting material derived from a polyHIPE through carbonisation[47] even with full retention of the pore structure.[48,49] Hereby the polymer is heated above 700°C in an inert atmosphere for a prolonged period of time. The only drawback is that the material often requires a chemical modification prior to heating because the unmodified samples tend to lose their
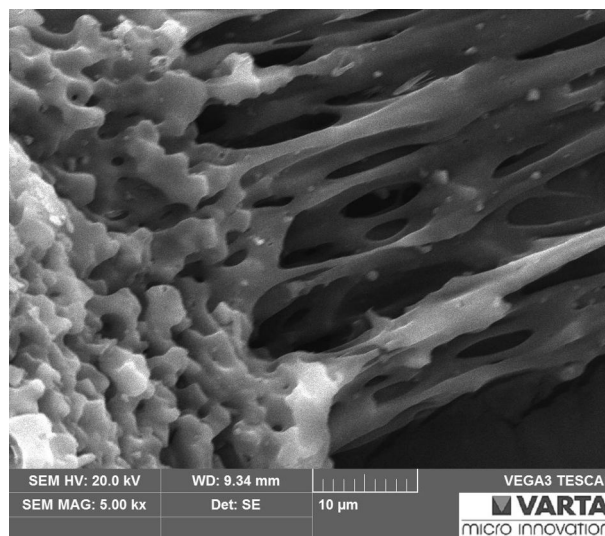
Figure 9: SEM of a collapsed porous structure

structure upon heating, thus collapsing into carbon chunks or undefined fibre-like structures which do not fulfil the requirements set for this work's application. However, the chemical modification is carried out by reaction of the foam with an agent, often meaning that the polymer foam has to be soaked with a reactive solution. A widely used modification is the introduction of sulfonyl groups[48,50,51] which can be difficult, especially when the reactant does not wet the polymer unaided. This problem can be avoided when the utilised polymer allows a gaseous modification like it has already been shown for polyacrylonitrile[52] (PAN), methacrylonitrile (PMAN)[53] or polydicyclopentadiene[54] (pDCPD). In these three cases it is sufficient to oxidise the

11

polymer in an air atmosphere, preferentially heating the samples to accelerate the process. In the well documented oxidative stabilisation of PAN[55,56] oxygen leads to additional crosslinks throughout the polymer, elevating its oxygen content and glass transition temperature.

3.3.3. pDCPD

DCPD which is shown in Figure 10 is produced as a byproduct in the steam cracking process of naphta, which significantly lowers its cost. When polymerised through Ring Opening Metathesis Polymerisation (ROMP) with
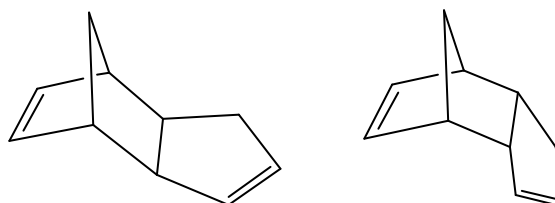
Figure 10: Dicyclopentadiene in its two forms

a suitable metalorganic catalyst it forms polymer chains which are crosslinked by opening the second unsaturated ring of the DCPD monomer.[57–59] Figure 11 shows the polymerisation into a rather hypothetical linear polymer chain (a) and the realistic, branching product (b).

Figure 11: Polymerisation and crosslinking of DCPD[59]

The highly crosslinked nature of polyDCPD makes it very durable in harsh environmental conditions. Due to its exceptional mechanical and chemical properties, this material has already been widely implemented in the fields of automotive and aerial exterior components, construction equipment, wash basins, containers for hazardous liquids, corrosion-resistant chemical process equipment, ballistic-resistant personal equipment[60] and many more.[61,62]

Kovačič, Krajnc and Slugovc have taken advantage of these assets of pDCPD and developed polyHIPE materials with very high rigidity and an inherently reactive character which allowed for an easy postpolymerisation modification of the foams.[54] The young's Modulus of these polyHIPEs was determined as 150 MPa at 80% porosity[63,64] which is twice as much as that of an equal polystyrene/divinylbenzene polyHIPE.[45,65]

3.3.4. pDVB

As mentioned in literature, one pathway to create a stiff polymer foam with a high glass transition temperature T_g is to use a convenient polymer of choice and treat it afterwards to modify its mechanical properties. For example, there is a possibility to produce a polystyrene (PS) foam and soak it in sulphuric acid to oxidise (and sulfonate) the polymer and thus elevate T_g to the desired value. Unfortunately the soaking process is rather complicated due to the dissimilar polarities of PS and sulphuric acid. The polar liquid has to be pressed into the nonpolar polymer by force, which produces moieties untouched and thus unmodified.[66]

Polydivinylbenzene can be seen as a relative to polystyrene. In fact it can be added to styrene to increase the T_g when needed, as it is the case in the present work. To withstand temperatures required for conversion of the embedded xanthates, the pHIPE matrix has to retain the shape it has received during polymerisation. The same applies to carbonisation. This means that in order to retain its morphology during thermal treatment, T_g has to be higher than the temperature of decomposition.

For styrene-divinylbenzene copolymers, studies on the dependence of T_g on the crosslink density show an exponential correlation between the two.[67] Aforementioned study assesses the best fit equation as

$$T_g(n) = 374.7 \cdot \frac{1 + 4.49}{n - N_{rot}}$$

where n is the number of styrene units in between the divinylbenzene (DVB) crosslinks. The fit equation is depicted as the continuous line in Figure 12.
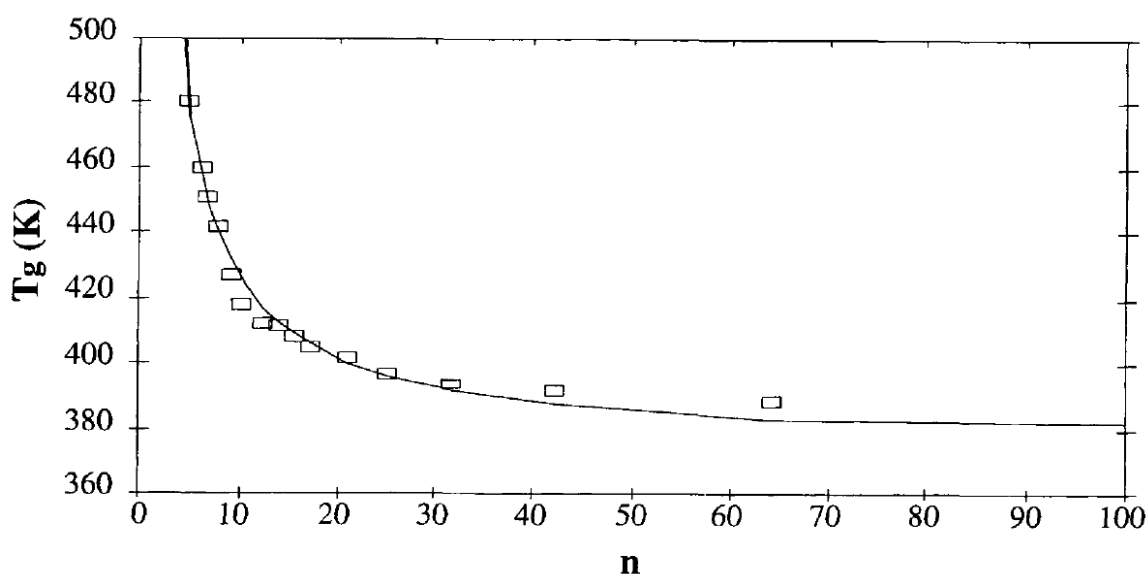

Figure 12: Glass transition temperatures T_g observed for styrene-divinylbenzene copolymers[67]

To achieve highest possible stiffness during thermal treatment of the resulting polymer, the crosslink density has to be as high as possible. Because of the good polymerisability of pure DVB, the option arises to use sole technical grade DVB as monomer, which is very convenient, because it is commercially available and eliminates the need for dilution of the monomer as a source of error. The 20% impurity consists (mainly) of ethylvinylbenzene (EVB) which is polymerised as well but cannot generate any crosslinks and thus generates

$$n = \frac{0.2}{0.8} = 0.25$$

Of course this means that on average there should be one EVB unit after every four DVB units.

Though usage of technical grade DVB with 80% purity actually produces a copolymer of DVB and EVB, nonetheless for simplicity reasons the polymer shall be referred to as poly divinylbenzene or pDVB.

3.4.   Nanocomposites

Formerly restricted to carbonanotubes and buckyballs, nanoscience has expanded into various fields of organic and inorganic chemistry, as well as merging the two fields through the development of hybrid materials which incorporate both: an organic polymer matrix and inorganic particles distributed throughout the bulk of it. The introduction of nanoparticles into polymers provides the latter with formerly non present properties, whereby the shape, size and composition of these particles has a significant impact on the properties of the resulting composites.[68,69]

There are two general methods for the incorporation of nanoparticles into the bulk of a polymer to create a nanocomposite: in situ polymerisation one the one hand, and ex-situ preparation with melt-compounding on the other.[70,71] The latter is basically a mixing process where inorganic particles are mixed into a molten polymer mass.[72,73] This process, obviously, is restricted to thermoplasts as matrix materials and has a number of further restrictions. The method of in situ polymerisation however, allows the usage of a wide field of polymers as long as the chosen nanoparticles do not interfere with the polymerisation process, and are dispersable inside the monomer. In this method, the particles are dispersed in the monomer, or a monomer solution, which is then polymerised, entrapping the particles in between the polymer chains[74-76] like it is depicted in Figure 13
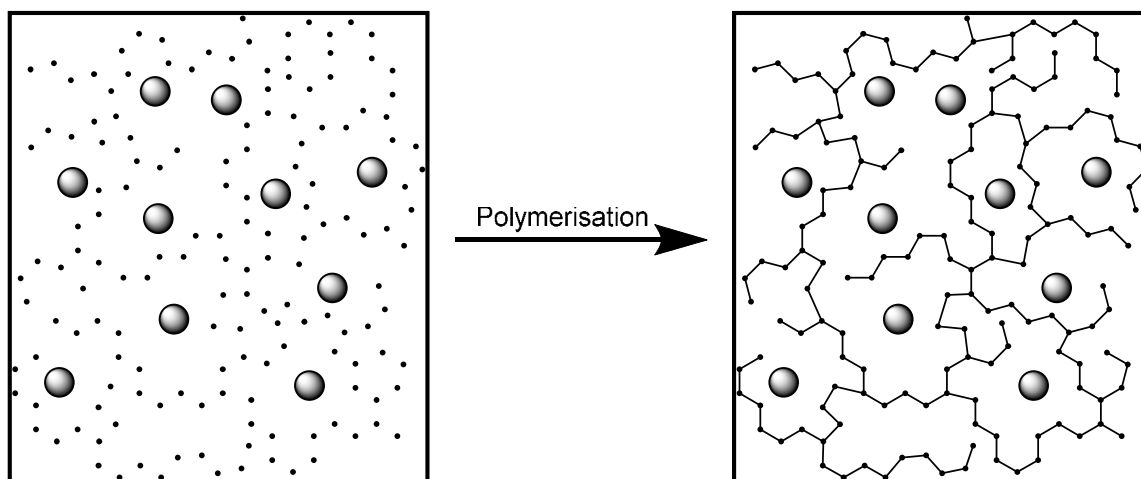
Figure 13: Schematical depiction of how particles or molecules are enclosed inside a polymer

Distributing the nanoparticles evenly throughout the polymer is essential for its homogenous properties in both cases, which in some cases is opposed by agglomeration processes. To prevent these, the surfaces and interfaces have to be modified by means of introduction of additives, change of the components, or surface chemistry.

These issues can be circumvented through the usage of suitable precursors instead of the materials themselves. Through resolving of the precursors in the monomer and entrapping them during polymerisation just like in case of the basic method, the precursor molecules are distributed by molecule throughout the final polymer. Since these are precursor molecules, they can be converted inside the polymer, yielding a species that otherwise would require significantly more effort to incorporate properly. As described in more detail in section "3.2 Xanthates as Precursors" and by other researchers of our institute[28,54,77,78] entrapped xanthates yield sulphide moieties throughout a polymer upon heating.

In case the in situ polymerisation fails, there is the option of a postpolymerisation modification. This can involve the covalent bonding of molecules to the substrate, or a mechanical introduction of substances into the polymer.[79] In other terms, the polymer is soaked in a solution consisting of a substance that has to be introduced into the bulk, dissolved in a solvent that can make the polymer swell. When the polymer soaks in the solution it swells, and the dissolved substance enters the network of polymer chains. When the solvent is evaporated, the substance remains inside the bulk and may be treated as one pleases.

4. Results and Discussion

4.1.   Solubility and polymerisation studies

In order to assess possible metal contents in a future polymer matrix, and to decide which metal xanthate to use for the preparation of a model system, the solubility of several already accessible metal xanthates in potential monomers was examined. After the preparation of saturated monomer solutions, the latter were dosed with a suitable catalyst and placed in an oven at 80 °C for 30 minutes.

The studies were performed in 1.5 mL glass vials with screw caps. with monomer amounts of 0.5 - 1.0 mL each. 0.5 mL monomer were placed in a vial with a small stirring bar. The weight of the vessel (including screw cap and stirring bar) was noted beforehand. Then a small amount of xanthate was added with a small spatula, and the combined weight was noted. After complete dissolution of the xanthate, another portion was added in the same manner. When the xanthate stopped to dissolve, another 0,5 mL of monomer were added, and the addition of xanthate was repeated as before.

4.2.1. Solubility in DCPD

Beneath in Table 2, the results are given for the performed solubility and polymerisability studies with dicyclopentadiene (80%, technical grade).

Table 2: Solubility studies with DCPD

Xanthate	Solubility [%]
$NiHep_2$	< 0.05
$BiHex_3$	< 0.05
$ZnEt_2$	< 0.05
CuHep	< 0.05
$InHep_3$	< 0.05
$CdHep_2$	< 0.05
$ZnHex_2$	< 0.05

Apart from low solubility of xanthates, no polymerisation occurred upon addition of catalyst M2, suggesting that the catalytic polymerisation is not possible. Due to the

extremely low solubility, the possibility of a catalytic polymerisation of xanthates in DCPD solutions was not further investigated.

4.2.2. Solubility in DVB

Beneath the results are given for the performed solubility studies with divinylbenzene (80%, technical grade). Table 3 shows the xanthate contents of the produced concentrated solutions in DVB.

Table 3: Solubitily studies with DVB

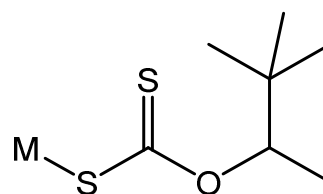| Xanthate	Solubility [%]
InHep$_3$	19 ±2
CdHep$_2$	16 ±1
GaHex$_3$	12 ±1
InHex$_3$	11 ±1
BiHex$_3$	7.8 ±0.5
PbHep$_2$	7.2 ±0.5
ZnHex$_2$	7.0 ±0.5
NiHep$_2$	5.8 ±0.5
SbHep$_3$	4.8 ±0.4
ZnHep$_2$	2.0 ±0.5
GaHep$_3$	0.9 ±0.3
CuHex	0.8 ±0.3
MnHep$_2$Phen	0.6 ±0.2
ZnEthyl$_2$	0.4 ±0.2

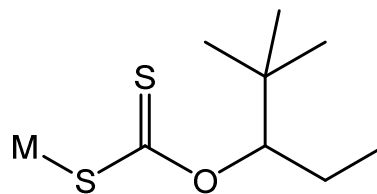**Figure 14: Metal hexyl xanthate, -Hex**

Figure 15: Metal heptyl xanthate, -Hep
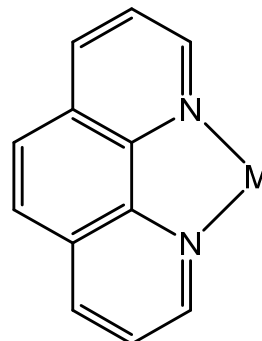
Figure 16: Metal phenantroline, -Phen

After addition of approximately 5 mg of dibenzoyl peroxide (DBP) as Initiator, the samples were placed in an oven at 80 ℃. After 30 min all samples with exception of CuHex were polymerised. The CuHex solution changed from bright yellow to dark brown, which is presumed to be an effect of the copper central atoms changing from the oxidation state of +1 to +2 and entering various side reactions alongside, which were not investigated any further.[80]

Figure 17: Polymerised xanthate solutions and unpolymerised CuHex solution

4.2.   Finding the right formulation of pHIPEs

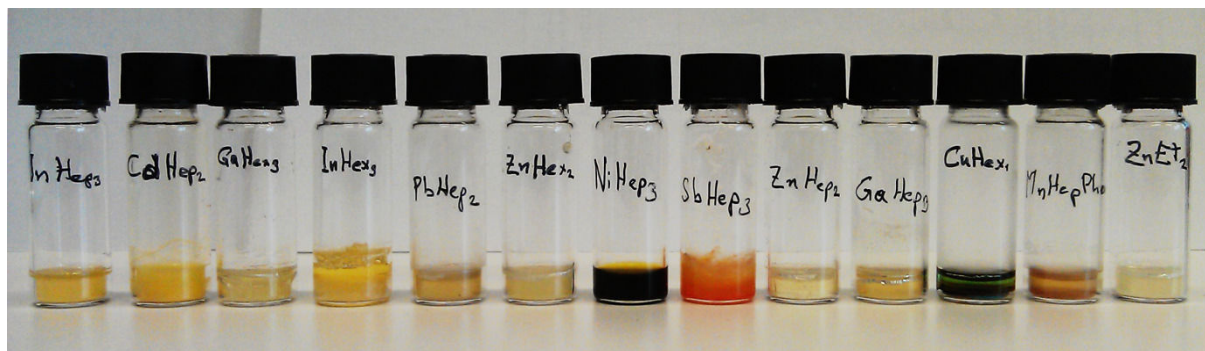The formulation of the polyHIPEs was based on Patent EP0060138B1 from Unilever,[44] however, it was adapted to the task at hand.

To determine a suitable composition and drying conditions as well as a way to remove the surfactant, experiments were conducted in an iterative manner.

Furthermore, various trials were conducted to determine the optimum conditions for curing and subsequent removal of surfactant and residual salts, so that the produced samples would be also suitable for further testing of thermal treatment methods.

The composition was varied in terms of porosity (internal-external phase ratio), salt content in the internal phase, initiator content and type. Surfactant content was set to 10% and monomer content to 20% as it appeared to be the composition which combined both high mechanical stability and porosity as well as an opportunity to still have a moderate amount of precursor molecules in a limited volume.

In order to remove the surfactant, the samples were removed from the mould, quickly rinsed with distilled water to remove glass shards, and immersed in the solvent or solvent mixture to be tested for several hours. Trials were

Figure 18: Examples of specimens cracked after swelling. The grid size is 5 mm.

performed with acetone, diethyl ether, dichloromethane, water and mixtures thereof. Water, salts and surfactant were expected to diffuse out of the sample into the washing solvent when possible.

Several formulations led to cracks in the samples as illustrated in Figure 18. The cracks appeared in samples with a thickness higher than a few millimetres. Trials

were first performed on pHIPEs without any xanthate loading and showed that a "dual-cure" method provided the pHIPEs with the desired properties. The selected treatment provided enough mechanical stability to withstand contractions of the sample upon drying, so that it did not crack during the evaporation of the washing agent.

In the mentioned dual-cure approach, dibenzoyl peroxide (DBP) is added to the continuous phase and ammonium persulphate (APS) is added to the internal phase. Such distribution of initiators provides a start of a polymerisation reaction from inside the bulk, while APS starts polymerising the interface, forming a membrane at the interface and quickly stabilising the emulsion.

To investigate the suitability of solvents for the purpose of surfactant removal, samples were immersed in 100 mL of the particular solvent (or mixture) in a covered glass beaker and left for several hours to let the diffusion do the work. Afterwards the samples were retrieved and placed on a dry paper towel until full evaporation of the solvent. The utilised solvent in the beaker was then evaporated and the residue was visually examined for salt and surfactant content.

Unsurprisingly, in cases of acetone, diethyl ether and dichloromethane the residue contained some amount of surfactant but no salt. In case of water the residue had some salt content, but no surfactant. A 1:1 mixture of acetone and water proved to be the most fitting washing agent, because it was able to extract both salt and surfactant, but to a significantly lesser extent than each of the two components by themselves. The use of diethyl ether was discarded due to its high evaporation rate, and dichloromethane because of its toxicity, and furthermore, both were unsuitable because of their inmiscibility with water.

Subsequent studies were conducted with xanthate loaded samples. Herein, acetone was found to dissolve the xanthates which were loaded into the pHIPEs, thus making it unsuitable for the desired application. Because of the above findings and also because the surfactant is supposed to leave the polymer during subsequent thermal treatment, the removal of surfactant was neglected in experiments conducted later on.

The final composition reads as follows: Span 80, DVB, and DBP were placed in a three-necked round-bottom flask and stirred with an overhead stirrer at 500 rpm for approximately 5 minutes until complete dissolution of DBP. The aqueous phase was added dropwise during 10 min. After complete addition of the aqueous phase stirring

was continued for further 30 min. After switching off and removing the stirrer, the emulsion was quickly transferred into 20 mL glass vials with screw caps which served as moulds and placed in an oven at 80 °C for approximately 24 h. The resulting pHIPEs were retrieved by carefully breaking the vials without damaging the pHIPEs, and rinsed with deionised water to remove glass shards. They were then dried in an oven at 80 °C for another 24 h.

To produce samples of simple geometrical shape, the obtained pHIPEs were lathed into cylindrical shape by removing the upper and lower part of the moulded sample, thus obtaining cylindrical shapes with a diameter of about 24.8 mm and a height of 9,5 mm. The exact measurements are reported where they appear relevant.

SEM micrographs were taken to assure that a proper interconnected structure was created. Representative ones are illustrated in Figures 19 and 20. The investigation showed that the samples, indeed, possessed a highly interconnected nature and sufficient wall strength. Besides, no microcracks could be found on the samples.
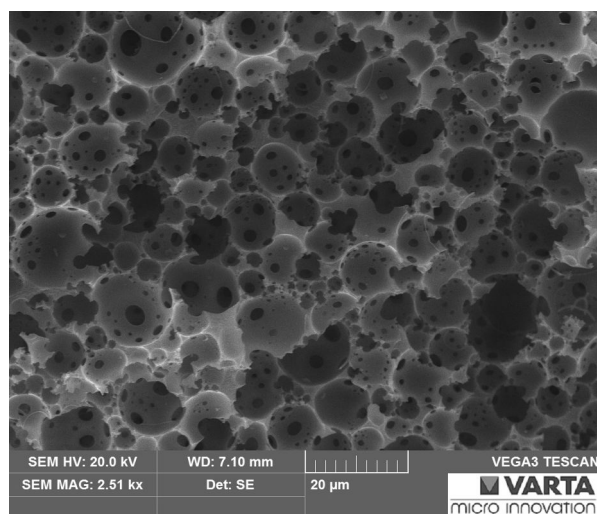

Figure 19: SEM of pDVB polyHIPE H08, no xanthate
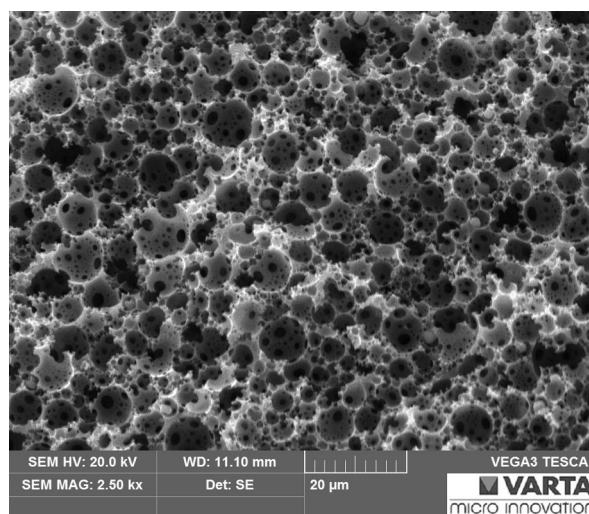
Figure 20: SEM of pDVB polyHIPE H31, InHep$_3$

As can be seen above, the xanthate loaded sample in Figure 20 has a lower pore diameter than the blank polyHIPE in Figure 19. This can be caused by the xanthate that itself acts as an additional surfactant in the system, and thus reduces the droplet size in the templating emulsion.

4.3.   Heat Resistance Testing

To investigate whether or not the produced polyHIPEs possess a glass transition temperature (T_g) high enough to withstand carbonisation, the samples were

examined in a simultaneous thermal analyser (STA) implementing thermogravimetric analysis (TGA) and differential scanning calorymetry (DSC).

A sample without xanthate loading (H08) showed a slight increase in weight on air which is most probably due to oxidation processes, which incorporate oxygen into the polymer as illustrated in Figure 21. In a Helium atmosphere the sample showed the approximate decomposition temperature deducted from the weight loss of the sample. The weight loss before that temperature can be accounted for by the loss of surfactant and unreacted monomer. Samples loaded with $InHep_3$ behave in a similar manner as the blanks which can be clearly seen in Figure 21.
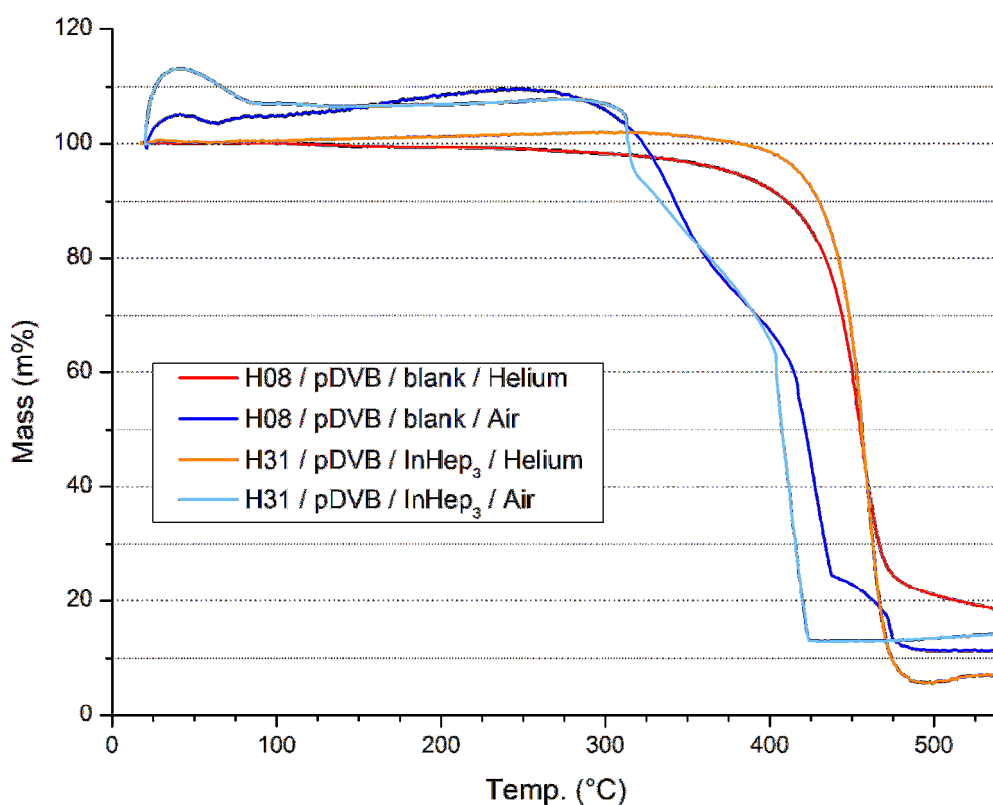
Figure 21: TGA of pDVB polyHIPEs H08 and H31 in air and helium atmospheres

DSC gives additional clues on the conversion temperatures of the xanthate as well as possible hints if supplementary oxidation may be required prior to carbonisation. As seen in Figures 22 and 23, the changes in weight are accompanied by corresponding energy flows which can be accounted for by the oxidation and evaporation processes taking place during thermal treatment. The DSC curves are represented as the dashed lines of the same colour as the TGA curves.

Unfortunately, the exact T_g could not be retrieved from the measurements, but since the knowledge of it being lower than required for a successful carbonisation

was enough at this point of this research, no further attempts to pinpoint it more accurately were attempted.

Figure 23 shows a difference in decomposition behaviours of the two samples in terms of energy intake. Sample H08 exhibits a higher energy intake upon decomposition which correlates with the endothermic nature of evaporation and some decomposition processes. Sample H31 however, shows a reduction of energy intake upon decomposition. This might point to with the catalytic activities of In_2S_3 which should have been formed during the heating sequence.
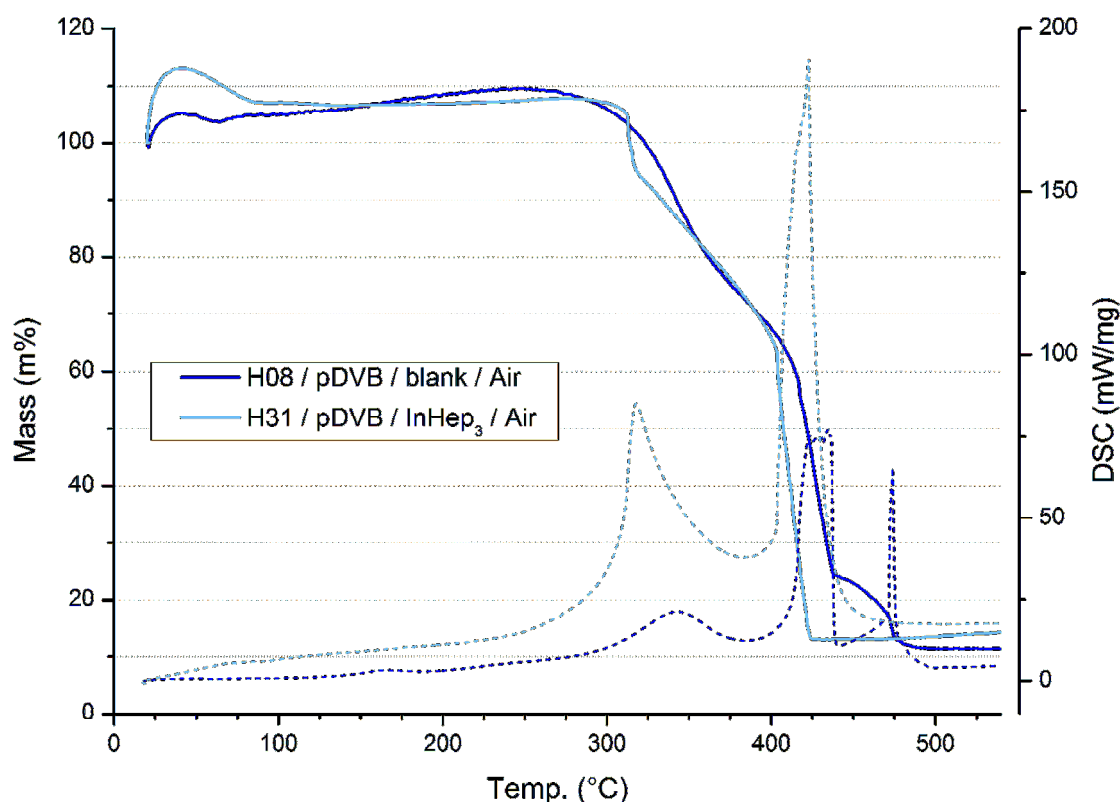

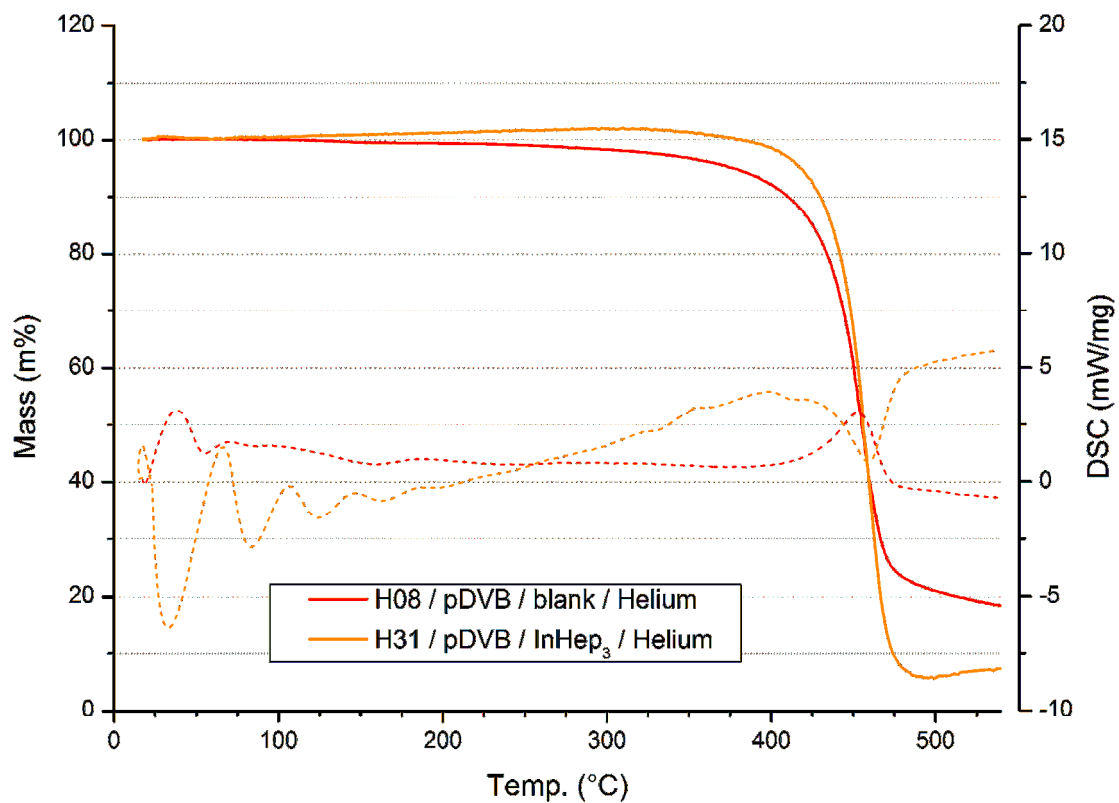**Figure 22: TGA and DSC graphs of pDVB polyHIPEs H08 and H31 in air atmosphere**

Figure 23: TGA and DSC graphs of pDVB polyHIPEs H08 and H31 in helium atmosphere

After thermal analysis of the samples, SEM micrographs were recorded to investigate the resulting structures.
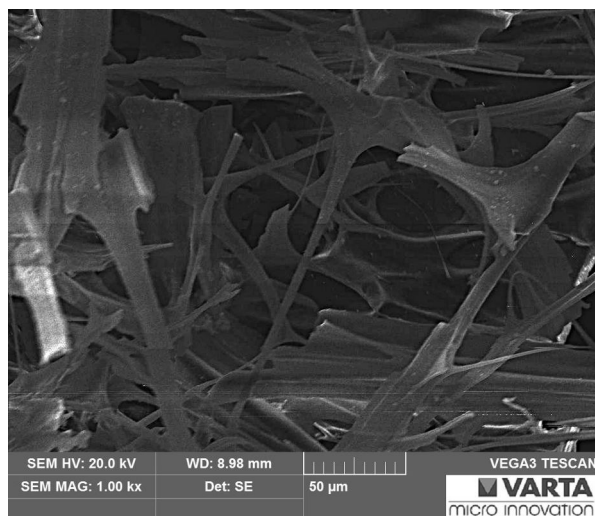
Figure 24: H08 after STA in helium atmosphere
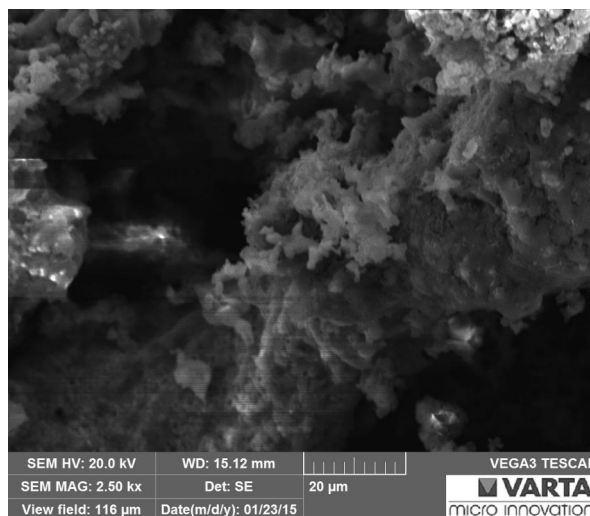
Figure 25: H08 after STA in air atmosphere
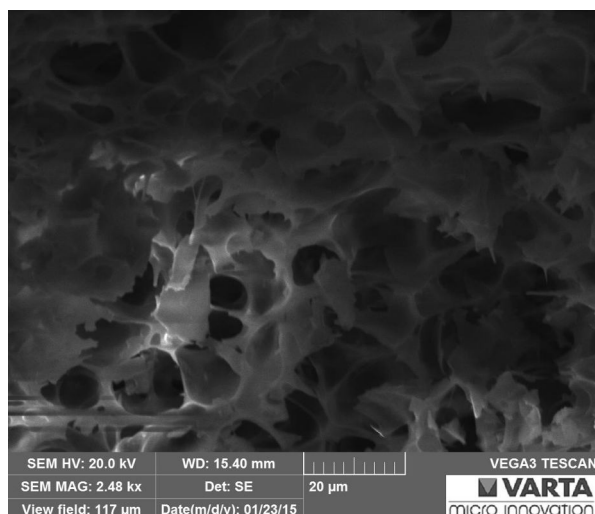
Figure 26: H31 after STA in helium atmosphere
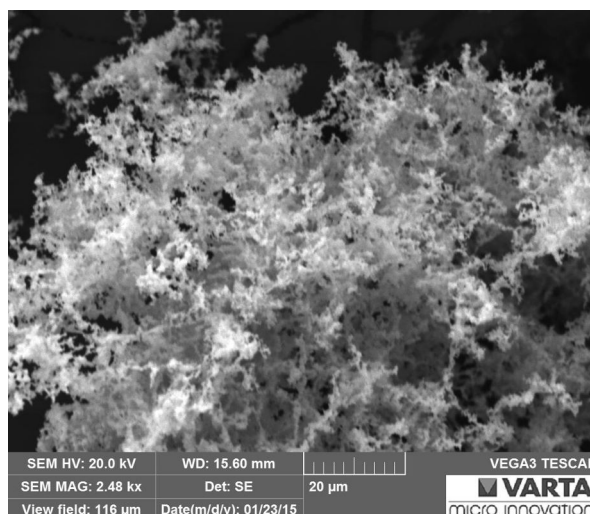
Figure 27: H31 after STA in air atmosphere

Generally, all four of the above Figures show that the samples H08 and H31 are not suitable for carbonisation without additional treatment. The resulting crosslink density proved to be insufficient to elevate T_g to higher values than the decomposition temperature of the polymer. However, when Figures 24 and 26 are compared, there is a difference in the manner of structure loss. While sample H 08 seems to have lost its structure completely, sample H31 retained a somewhat deformed, but still porous structure. A possible cause for that may be the additional crosslinks introduced through the xanthate decomposition reaction, as xanthates are well known crosslinking agents used in rubber industry.

The STA in air predictably resulted in nearly complete decomposition of the samples. H08 shown in Figure 25 completely lost its structure and was not analysed any further, however, the structure reminds of the ones found in certain types of activated carbon.[81,82] Due to the NaCl and $NaSO_4$ (from APS decomposition) inside the polymer, the sample did not decompose completely. When examined closely, the new structure of H31 remotely reminds of its former structure, but significantly smaller and highly cracked. While being handled during SEM sample preparation, it appeared white in colour and very brittle.

EDX analysis of sample H31 shown in Figure 27 gave the values shown in Table 4. As it was expected, the sample consists of mainly the organic residues of the polyHIPE. Judging from the atomic fractions of the elements, and considering the previously added constituents, the sample most probably consists of NaCl, $NaSO_4$, NaOH, In_2O_3, and moieties of unreacted carbon with carbonyl and hydroxy groups as they are found on the surface of activated carbon.[81]

Table 4: EDX analysis of sample H31 after STA in air

Element	Weight %	Atomic %
C	20.33	34.27
O	40.45	51.19
Na	8.24	7.25
S	3.46	2.19
Cl	0.62	0.36
In	26.89	4.74
Total	100	100

In addition, EDX of sample H31 proves that at least certain amounts of metals can be incorporated into polyHIPEs through the pathway of in-situ polymerisation, which is important information considering the rather low levels of metals inside the polyHIPEs due to the low solubility of xanthate in the monomers. Considering the given information, it can be said that it still is reasonable to conduct further experiments, despite the lack of hard evidence of sulphide formation.

4.4. Tempering

The information retrieved from STA in Chapter 4.3 *Heat Resistance Testing* revealed that the polymer matrix was able to withstand the temperatures required for a successful conversion of xanthates to sulphides without structure loss. Therefore samples were placed in a tube furnace at different temperatures and for various amounts of time under a nitrogen flow to create sulphide moieties inside the polymer as described in Chapter 3.4 *Nanocomposites*.

It shall be mentioned, that during the thermal treatment procedures, the high insulating nature of the samples should be minded. Due to the highly porous nature of polyHIPEs, they possess very low heat conductivity as does any other porous material. Therefore, the heating process has to be be slow enough to ensure that the temperature difference between the sample's centre and its surface is as little as possible, or that at least the dwelling time on the target temperature is long enough to ensure all chemical processes possible at the given temperature are completed and the sample is in a state of thermodynamic equilibrium.

Since STA suggests structure retention at temperatures well over 300 °C, the thermal conversion of xanthates into sulphides, as well as an oxidative modification of the polymer should be feasible in the porous polymer matrix without structure loss.
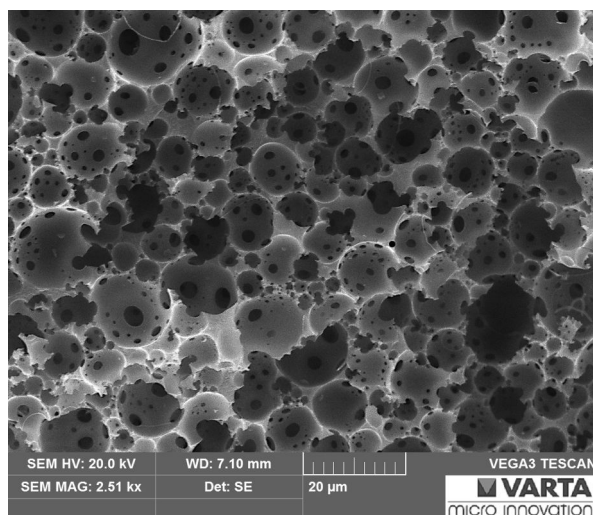
Figure 28: SEM micrograph of pDVB sample H08 before tempering (no xanthate loading)
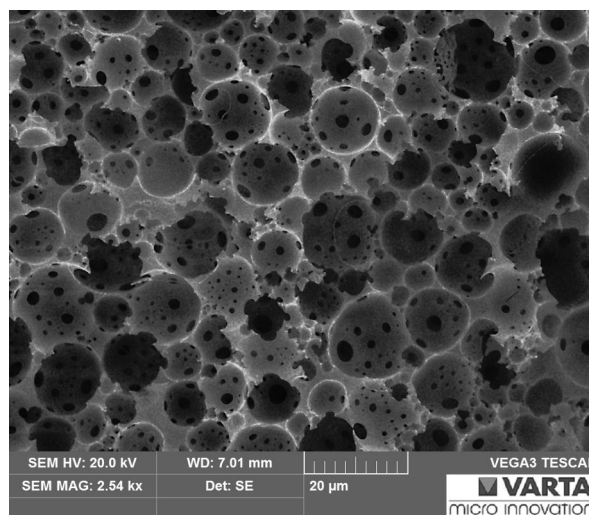
Figure 29: SEM micrograph of pDVB sample H08 after tempering for 2 h at 200 °C (no xanthate loading)

A polyHIPE sample without xanthate loading, namely sample H08, was tempered for 2 hours at 200 °C. Figures 28 and 29 show SEM micrographs recorded before and after the tempering process. There it can be seen that the structure was retained to full extent. Samples that were treated in later stages of this work were also

controlled on the matter of structure retention, and showed no change whatsoever. Hence it was deemed unnecessary to illustrate all of the micrographs regarding the absence of morphological change in later parts of this work, keeping to illustrations of altered morphology only.

A detailed documentation on the performed thermal tests is given in Table 21 on Page 56. Values of said table indicate a certain mass loss of about 3 - 5% during the tempering process. The loss cannot be unequivocally attributed to neither the xanthate decomposition reaction, nor the evaporation of other components alone. Assuming a total absence of water in the samples at hand, they contain three components that are prone to evaporation in the given conditions: surfactant, residual monomers and xanthate decomposition products. The latter are of utmost interest. However, attempts at quantification are not reasonable as every one of the aforementioned components is partially entrapped in between the polymer chains, and therefore cannot be removed from the compound completely. Furthermore, the surfactant Span 80, which was used in the samples, is not a single substance, but a mixture of several components, the specified ingredient sorbitane monooleate accounting for only as little as ≤60% of the compound according to the manufacturer's website,[83] being accompanied by esters of fatty acid of lower and higher mass, which evaporate accordingly at lower or higher temperatures. Additional research performed on the composition suggests that the real composition not only contains significant amounts of other mono- fatty acid esters, but also contains large portions of di- tri- and tetraesters as well as various free fatty acids.[84,85]

To evaluate the intercalated sulphide moieties after tempering, X-ray powder diffraction analysis (XRD) was applied since it is known for sulphides to be visible in polymers.[78,86]

The samples were ground into powder using a porcelain mortar and pestle, then measured by XRD. Spectra of the two samples alongside the reference spectra are shown in Figure 30.
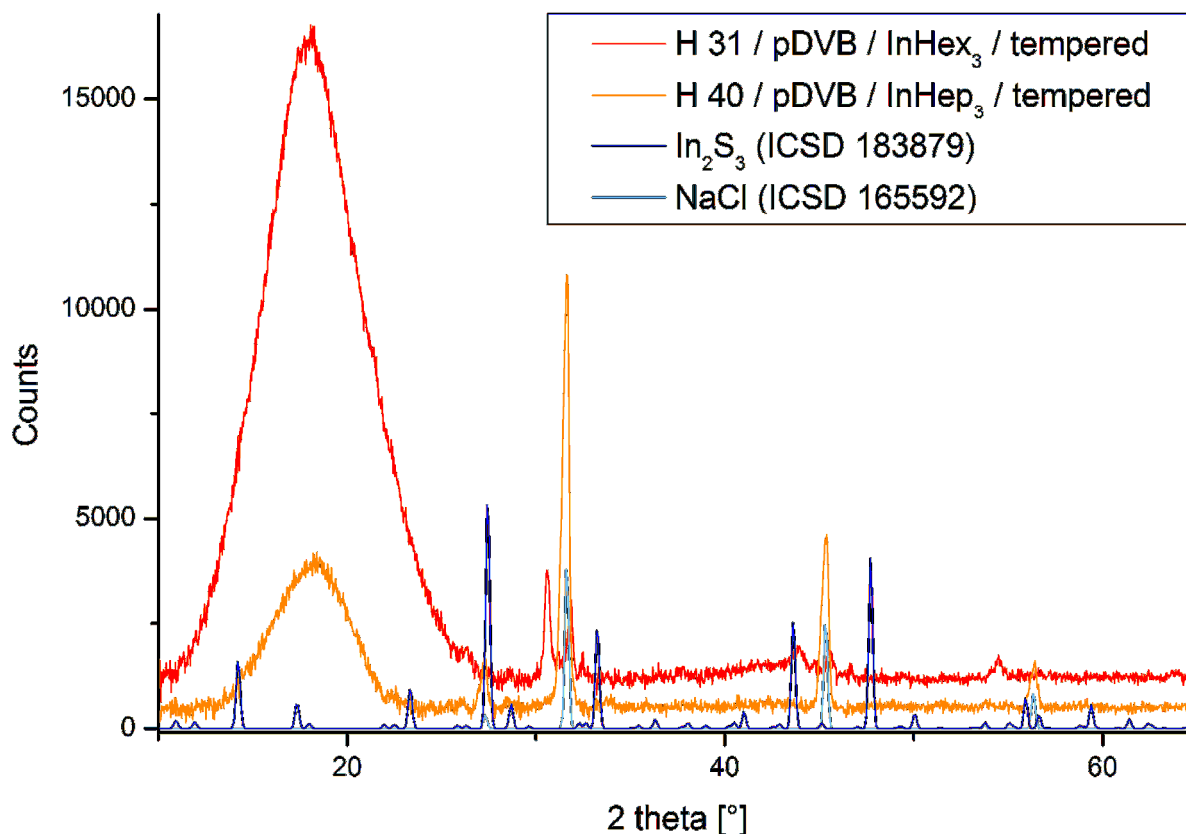
Figure 30: XRD spectrum of xanthate loaded pDVB polyHIPEs H 31 and H 40 after tempering

Except for the residual NaCl of the internal phase, not much data of interest is to be found in the spectrum. Reasons for this can be threefold. One possible reason could be a failed sulphide formation. Another reason could be the formation of amorphous indium sulphide which would be invisible to XRD since this method relies on the presence of crystalline moieties. The last possibility is that the resulting concentration of In_2S_3 in the sample is below the detection limit.

In_2S_3 is being formed reliably from both $InHep_3$ and $InHex_3$. Figure 31 depicts In_2S_3 formed from pure, powdered $InHep_3$ to compare it to a sample graph from Inorganic Crystal Structure Database[87] (ICSD). The

Figure 31: XRD of In_2S_3 formed from pure $InHep_3$

crystallite size was found to be 10 nm through peak width correlation using the Scherrer-equation.

Arithmetically determined sulphide concentrations of four selected polyHIPEs are presented in Table 5, which shows that the expected contents range from

29

1.19 to 6.10% of dry sample mass, depending on the sulphide type and on processes anticipated during tempering. The sulphides calculated with, were In_2S_3, Bi_2S_3, CdS and NiS, being the most common and stable types of sulphides of the corresponding metals.

Table 5: Calculated xanthate, metal and sulphide contents in polyHIPEs

Xanthate	M_{Xan} [g mol^{-1}]	M_{Metal} [g mol^{-1}]	m%$_{Xan}$ [%]	m%$_{Me}$ [%]	atom%$_{Me}$ [%]	m% Sulphide
InHep$_3$	688.80	114.82	19.06	2.67	3.49	4.00 - 4.71
InHex$_3$	646.72	114.82	17.75	2.22	2.52	2.90 – 3.21
BiHex$_3$	740.88	208.98	7.78	2.19	1.35	2.70 - 2.84
CdHep$_2$	495.07	112.40	16.61	3.77	4.20	4.85 - 6.10
NiHep$_2$	441.35	58.71	5.81	0.77	1.69	1.19 - 1.47

Calculations were carried out with following formulas, whereas the abbreviations are explained below them.

$$m\%_{Me} = \frac{m\%_{Xan}}{M_{Xan}} \cdot M_{Me}$$

$$m_1\%_{Me_xS_y} = m\%_{Me} + \frac{m\%_{Xan}}{M_{Xan}} \cdot M_S \cdot \frac{y}{x}$$

$$m_2\%_{Me_xS_y} = \frac{\left(m\%_{Me} + \frac{m\%_{Xan}}{M_{Xan}} \cdot M_S \cdot \frac{y}{x}\right)}{\left(m\%_{Me} + \frac{m\%_{Xan}}{M_{Xan}} \cdot M_S \cdot \frac{y}{x} + (100 - m\%_{Xan})\right)} \cdot 100\%$$

$$mol\%_{Me} = mol\%_{Xan} = \frac{m\%_{Xan}}{M_{Xan}}$$

$m\%_{Xan}$ ... mass percentage of xanthate in xanthate / DVB solution

$m\%_{Me}$ ... mass percentage of metal in the resulting polyHIPE

M_{Xan} ... molar mass of xanthate

M_S ... molar mass of sulphur (32.064 g mol^{-1})

$m_1\%_{Me_xS_y}$ ... lower calculated sulphide content in tempered polyHIPE

$m_2\%_{Me_xS_y}$ ... upper calculated sulphide content in tempered polyHIPE

$mol\%_{Me}$ ... molar percentage of metal in untempered polyHIPE

$mol\%_{Xan}$ ... molar percentage of xanthate in untempered polyHIPE

The upper and lower values of the sulphide contents depend on which processes are considered during tempering. As described before, in Chapter 3.2 *Xanthates as Precursors* on page 8, xanthates decompose, releasing mainly gaseous products

when heated in nitrogen atmosphere. However, since xanthates are known to be responsible for crosslinking in rubber, they might as well remain covalently bonded inside the polymer. Thus the upper value results from the assumption that all volatile compounds have left the sample and have reduced its weight while the amount of sulphide remains constant. The lower value originated from a mechanism where the sample retains its original weight, and decomposition of xanthate moieties are assumed to involve only in creation of additional crosslinks in the polymer since xanthates are known to be used as crosslinking agents in the rubber industry.[8]

As can be seen in Table 5, the sulphide contents are close to the detection limit of XRD, which is about 2% of the sample[88] or even less. It is commonly known that as the particles of the analyte get smaller, the reflection peaks grow broader. Considering the fine distribution of xanthates throughout the polymers, the created sulphide particles should be even smaller than the particles analysed in Figure 31, thus resulting in an even broader peak at lower intensities. Paired with the presence of at least a certain amorphous portion, the peaks plainly disappear in the noise and cannot be made visible.

A hope for further experiments lies in the mass loss during carbonisation. Considering a constant amount of sulphide, the polymer matrix loses a great portion of its mass, thus elevating the percentage of sulphide in the carbonised compound.

4.5.   Oxidative Treatment

To enhance the glass transition temperature of the polyHIPEs, latter were subjected to an oxidative treatment in air. Samples were placed in a tube furnace at different temperatures until satisfactory results were obtained. The oxidation processes start at rather low temperatures, thus limiting the temperature of oxidative heat treatment to the point where uncontrolled burning would start due to excess heat generation. Temperature values in the experiments were chosen based on empirically realistic values obtained from STA experiments described in Chapter 4.3 Heat Resistance Testing on Page 22.

As expected, the samples turned out to start burning from the inside when the temperature was too high, resulting in blackened areas in the centre of the sample as depicted in Figure 32 in the middle. Due to the good insulating properties, reaction heat from the oxidation could not be dissipated quickly enough from the centre of the samples, but the porous interconnected structure allowed for enough convection of

oxygen for the sample to burn for a certain time. In those cases, the shrinkage process was too local, which made the samples break from inside-out as can be seen in Figure 32, middle and right. A thinner sample which had a thickness of 5 mm instead of over 9 mm like the others was found not to be affected by these problems to the same extent.
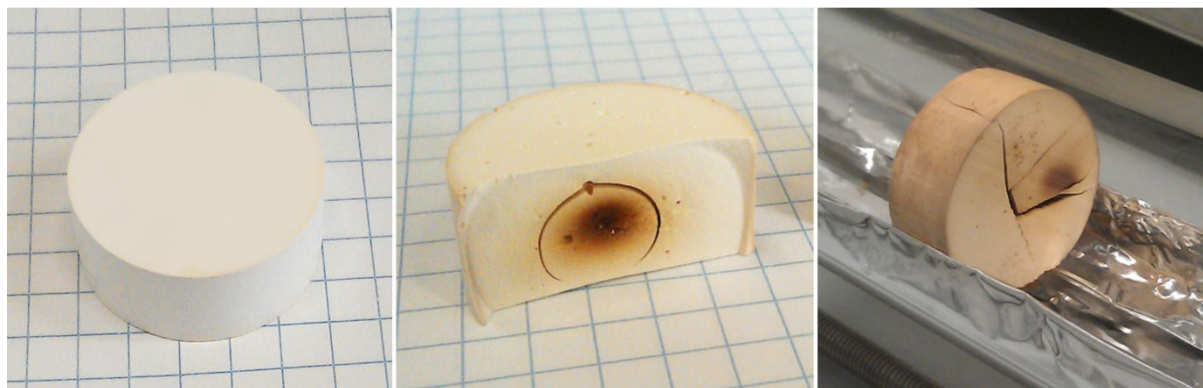
Figure 32: Sample shapes; left: shape of lathed sample before oxidation; middle and right: samples burned and cracked; grid size is 5 mm

After several trials, the optimum temperature for oxidative treatment was found to be 110 °C for samples with a diameter of 25 mm, a thickness of 9 - 10 mm, and a porosity of 80 %, however, thinner samples withstand higher temperatures. As mentioned before, a detailed documentation on the performed thermal tests is given in Table 21 on Page 56.

The samples gained weight during the oxidative treatment, which can be accounted for by an incorporation of oxygen into the polymer, as expected. However, the values are hardly quantifiable due to the possible simultaneous evaporation of other compounds, as explained earlier in the Chapter 4.4 *Tempering*.

The oxidatively treated samples were investigated via SEM to assure of retention of the porous structure. The micrographs revealed that no morphological changes had occurred when compared to the untempered or unoxidised structures.

4.6.   Carbonisation

After an oxidative treatment, samples were placed into a tube furnace in nitrogen atmosphere and heated to higher temperatures of 430 and 500 °C to investigate the structure retention capabilities. Sample H38_I, a sample without xanthate loading, was submitted to the previously described heat treatments, namely tempering, oxidation and carbonisation, to assess the impact of carbonisation on the samples.

The sample shrank greatly, and was partially disintegrated, but retained representative regions which could be analysed. The frame to the right in Figure 32 shows sample H38_I after oxidation. Figure 33 depicts the same sample after further tempering at 430 °C in nitrogen atmosphere. While cracked, but nonetheless a monolith in Figure 32, in Figure 33 it is shattered into four pieces, as predicted by the cracks. Samples already start to lose weight and change colour at this temperature.

Figure 33: Disintegrated sample H38

A major concern at this moment was that the sample would melt upon carbonisation due to the residual salts and surfactant inside the porous structure as it is the case with PMAN,[53] though as it turned out, this was not the case. The sample shrank a little in size and mass, and cracked at several places. Figure 34 depicts the shard of sample H38_I prior to, and after carbonisation. The right frame was graphically enhanced in order to visualise the cracks in spite of bad contrast conditions of the middle frame.

The various cracks of the carbonised sample could originate either from an excessive heat rate, which was as high as 4 °C/min or from an unfitting pretreatment.
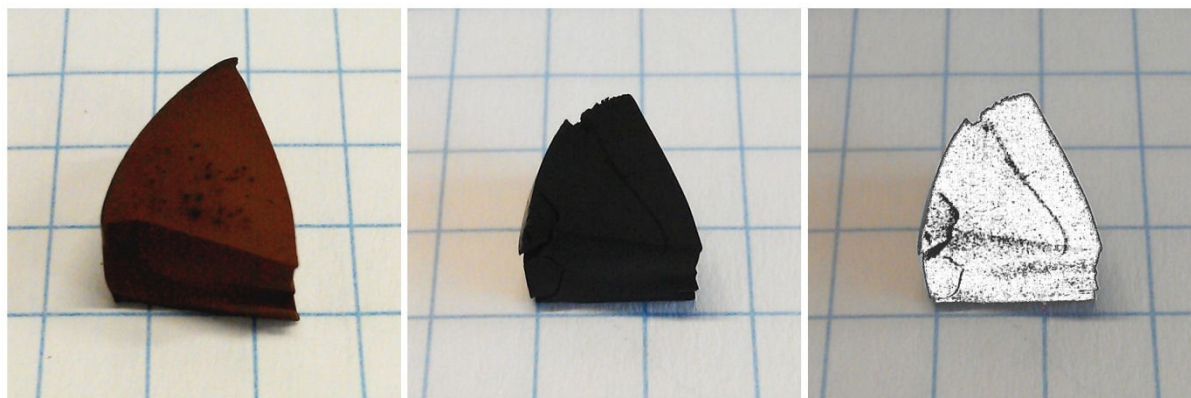
Figure 34: Shard of sample H38_I, the grid size is 5 mm; left: after tempering at 430 °C, middle: after carbonisation at 900 °C; right: enhanced image of middle frame

Sample H40_II was treated in a similar manner, although the oxidation and pre-carbonising steps were carried out at temperatures of 110 and 500 °C respectively. The sample did not evolve any cracks, but shrinkage occurred to a greater extent in the middle of the sample, resulting in a thinned out centre and a thicker perimeter. To acquire the SEM image seen in Figure 35 at this stage, a small shard was broken off the outer rim of the sample. The structure appears to be still intact, the only change in shape being the thinned out walls.

Furthermore, EDX at this stage reveals a significant difference in atomic composition between the sample's bulk and its outer shell. The results given in Table 6 demonstrate a significant difference of indium contents between the two regions. Where the bulk gives only a slight signal for indium that is scraping on the machine's detection limit, a low but solid indium signal accounting for approximately 1% of the sample's

Figure 35: SEM micrograph of Sample H40_II after 500 ℃ pretreatment

mass can be recorded at its outer shell. Signals for sodium and chlorine are also higher, but could be the result of sample contamination.

Table 6: EDX analysis of Sample H40_II after 500 ℃ pretreatment

Position:	Outer Shell		Bulk	
Element	Weight %	Atomic %	Weight %	Atomic %
C	80.29	88.58	83.88	91.24
O	7.17	5.94	5.08	4.15
Na	4.76	2.75	3.11	1.77
S	3.04	1.26	0.86	0.35
Cl	3.60	1.35	6.64	2.45
In	1.14	0.13	0.44	0.05
Total	100	100	100	100

After carbonisation at 900 ℃ the central part becomes even shallower than before, hinting at an uneven distribution of oxygen throughout the sample. When broken in half, the central part appears slightly glossy, which can be observed in the left frame of Figure 36. To improve visibility of the sample, a graphically enhanced version is depicted in the middle frame of the same Figure. The cross-section of sample H40_II is to be found in the right frame of Figure 36, and reveals how much more the centre shrinks in comparison to the perimeter. The shape has been traced from a picture, meaning that the irregularities in the figure are not handmade, but rather that the sample has shrunk irregularly.

Figure 36: Sample H40_II broken in half after carbonisation at 900℃, grid size is 5 mm; left: original image; middle: enhanced image of left frame; right: contours of sample's cross-section with measurements

The glossy shine is a sign of smooth surfaces, whereas the dull ones are rough. This observation is confirmed later in the SEM micrographs. At this point, the sample has developed a certain amount of conductivity which is enough for the sample to be measured in SEM without prior gold coating. When investigated via SEM, the sample featured several types of structures, ranging from a typical polyHIPE structure, to a molten but nonetheless porous appearance.

In Figure 37 can be seen that the walls in between the pores have lost much substance, while the pores themselves have seemingly not shrunk at all when compared to Figure 35.

The inner regions of the sample exhibit the greater a loss of structure, the closer the region is located towards the centre, which can be observed in Figures 37 to 38. The micrographs in Figures 39 and 38 are taken from the centre of the sample, whereas the one from Figure 40 is from approximately 3 mm towards the perimeter.
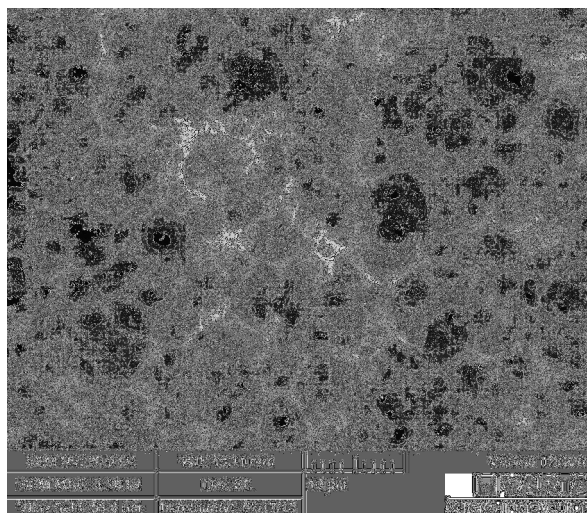
Figure 37: SEM micrograph of H40_II peripheral region after carbonisation
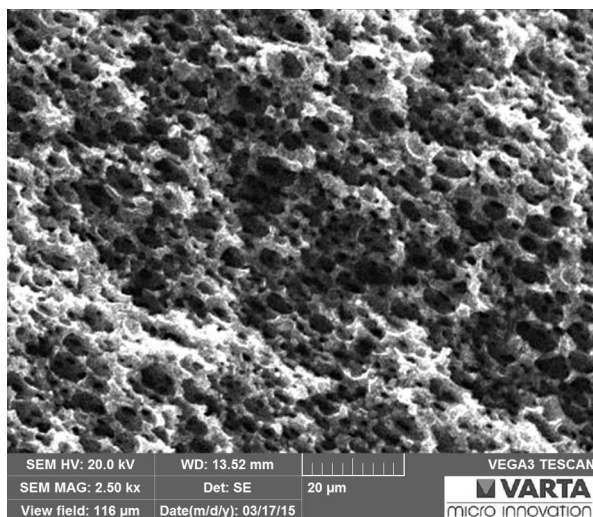
Figure 40: SEM micrograph of H40_II from the mean region
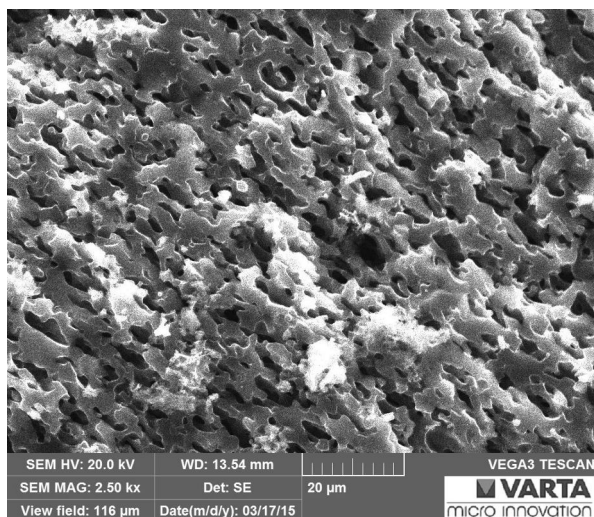
Figure 39: SEM micrograph of H40_II from the central region

Figure 38: SEM micrograph of H40_II from the central region in higher magnification

As it can be observed in these micrographs, the sample loses its structure to some extent, but the different regions exhibit different behaviour during carbonisation. Judging from the patterns in Figures 39 and 38, the T_g of the polymer was exceeded in that region, whereas in the peripheral region depicted Figure 37 the material's T_g was sufficiently higher. Due to the meltdown of the material, the pores collapsed in central parts of the sample, and the walls fused together, resulting in thicker walls with smaller pores. Apparently the deformation process also takes place in the region depicted in Figure 40, but either starts at a higher temperature, leaving the polymer less time to deform, or happens at a slower pace than in the central part.

Figure 38 depicts the same region as Figure 39, but in higher magnification. When observed, the cause of the glossy appearance described earlier becomes apparent. Due to the disproportionation of the pore/wall ratio, namely the decrease in pore quantity, and increase in wall thickness, fracture surfaces of the broken walls emerge facing roughly the same direction, which in turn manifests itself in a glossy appearance of the samples after fracture, and can be easily observed with the naked eye.

The observed difference in behaviour of different regions of the sample is most probably caused by an uneven distribution of oxygen during the oxidative pretreatment. It is apparent that the inner regions of the sample possessed a different composition before carbonisation, and therefore behaved differently during the process. The outer regions of the sample seem to have been oxidised to a higher degree than their centrally located counterparts, resulting in better shape-retention capabilities.

EDX analysis of sample H40_II reveals a curious pattern of indium content. As displayed in Table 7, indium content is highest at the sample's surface. There is also a small, barely measurable indium content in the centre, but the morphologically most attractive region, the perimeter, remains without a meaningful indium signal. The atomic ratio of indium to sulphur remains the same for both the shell and the centre, namely 1:16. The elevated indium content at the shell can be explained through the shell being the only part of the sample that was in direct contact with glass, producing an opportunity for xanthate molecules to arrange themselves along that interface, thus ending up in higher concentrations by the end of polymerisation.

The chlorine content has apparently disappeared completely from all three analysed regions during carbonisation, which is very convenient. Its former counter ion sodium remains in the compound.

Table 7: EDX analysis of Sample H40_II after carbonisation

Position:	Outer Shell		Perimeter		Centre	
Element	Weight %	Atomic %	Weight %	Atomic %	Weight %	Atomic %
C	55.02	65.15	92.64	95.53	90.39	94.13
O	30.00	26.67	3.78	2.93	5.29	4.14
Na	10.45	6.46	1.04	0.56	1.38	0.75
S	3.63	1.61	2.54	0.98	2.36	0.92
In	0.89	0.11			0.57	0.06
Total	100	100	100	100	100	100

The central region exhibits significantly lower oxygen content than the shell, which is probably due to oxygen reaching the inner regions to a lesser extent during the oxidation step, resulting in lower degrees of oxidation, the further away from the sample surfaces as described for the pDCPD system.[54] Additionally, residual oxygen which can remain in the porous structure during the supposedly inert heat treatment

steps can lead to further oxidation at the surface, since there is a temperature drop from the outside towards the inside of the samples during heating. When the residual oxygen is depleted in the outer regions, some more diffuses from the inside, and is thus fixated there until no oxygen is left in the system. Another cause for the elevated oxygen content is a photocatalytical oxidation during storage.

At the temperatures of the carbonisation step, metal sulphides of the type MS_x created through tempering may be oxidised to metal oxides of the type MO_x[78,89] which may occur preferably at the sample surface due to reasons mentioned above. However, there is no actual hard evidence of metal oxide formation from the acquired data.

During carbonisation, elements such as carbon, oxygen, sulphur and others are prone to leaving the sample, while several others tend to form stable inorganic compounds which are able to withstand high temperatures. Assuming sodium as the only element which does not leave the given samples, changes in contents of other elements can be assessed by normalising them to the sodium contents. The normalised values are given below in Tables 8 and 9.

Table 8: EDX analysis of Sample H40_II after 500 °C pretreatment, normalised to sodium contents

Position:	Outer Shell		Bulk	
Element	Weight	Atomic	Weight	Atomic
C	16.87	32.21	26.97	51.55
O	1.51	2.16	1.63	2.34
Na	1	1	1	1
S	0.64	0.46	0.28	0.20
Cl	0.76	0.49	2.14	1.38
In	0.24	0.05	0.14	0.03

Table 9: EDX analysis of Sample H40_II after carbonisation, normalised to sodium contents

Position:	Outer Shell		Perimeter		Centre	
Element	Weight	Atomic	Weight	Atomic	Weight	Atomic
C	5.27	10.09	89.08	170.59	65.50	125.51
O	2.87	4.13	3.63	5.23	3.83	5.52
Na	1	1	1	1	1	1
S	0.35	0.25	2.44	1.75	1.71	1.23
In	0.09	0.02			0.41	0.08

When compared to the EDX analysis of the sample after the preceding heat treatment step seen in Table 8, the shell's relative oxygen content raises greatly upon carbonisation, especially in the shell. The sulphur contents show a decrease, while indium contents seem to stay at roughly the same level.

To investigate, whether or not other xanthates behave differently, $BiHex_3$ containing Sample H29_III was tempered in the same manner as the samples before, and analysed with EDX. The results are given in Table 10.

Table 10: EDX analysis of Sample H29_III after tempering

Position:	Outer Shell		Bulk	
Element	Weight %	Atomic %	Weight %	Atomic %
C	84.49	88.23	94.47	97.51
O	14.84	11.64	2.06	1.59
Na	<0.01	<0.01	0.44	0.24
S	<0.01	<0.01	0.85	0.33
Cl	0.26	0.09	0.69	0.24
Bi	0.39	0.02	1.49	0.09
Total	100	100	100	100

EDX analysis shows that although the sample has a higher metal content, the difference is practically negligible, indicating that the approach towards sulfide and carbide loaded carbonaceous foams by means of polymerisation of saturated xanthate-in-monomer solutions may not be the best choice.

4.7.   Compression modulus

To evaluate and compare the mechanical properties of the polyHIPEs made, compressive mechanical tests were performed on the samples. The acquired

39

compressive moduli were then compared to literature values.[45,65] These are displayed in Table 11. All samples mentioned there were made with addition of 10% Span 80 based on the monomer.

Table 11: Mechanical properties of polyHIPEs

Sample	Density [g/cm^3]	E-Modulus [MPa]	Yield stress [MPa]	Yield strain [%]
H38, blank, untempered	0.20	84	5.0	5.9
H38, blank, untempered	0.20	80	5.1	6.5
H38, blank, tempered	0.20	85	5.8	7.0
H31, InHex$_3$ tempered	0.22	88	7.1	7.9
H39_III, blank, oxidised	0.22	101	7.5	8.7
H39_V, blank, oxidised	0.22	102	7.6	8.6
H40_I, InHep$_3$, tempered	0.19	84	6.3	8.7
PS/pDVB, reference**Fehler! Textmarke nicht definiert.**	0.22	186	6.3	?
pDVB, reference**Fehler! Textmarke nicht definiert.**	0.17	110	3.5	4

As can be seen in Table 11, the tempering process has little impact on the polyHIPE's elastic modulus, whether xanthate loaded or not. Oxidative treatment on the other hand leads to an increase of roughly 20%.

In comparison to literature, the obtained values appear rather modest. However, it shall be noted that these values were obtained from samples polymerised in different conditions, making it impossible to draw accurate conclusions from comparing these samples. Namely, the main differences from this work's preparative method were higher initiator content, lack of extra addition of electrolyte (NaCl), number of initiators used simultaneously, type of initiator, vessel and stirrer types. Furthermore, the pore diameters of the reference samples were estimated as larger than those produced in this work. The PS/pDVB sample had a pore size of 8-10 µm and the pDVB sample of 15-20 µm against pore sizes of this work varying in between 4-10 µm, depending on the sample.

4.8. Post polymerisation xanthate incorporation

Due to the dissatisfactory low xanthate loadings resulting from the in-situ polymerisation method described before, another route was tested. PolyHIPE samples were soaked in a concentrated solution of $InHep_3$ for seven days, dried at 80 °C in air and tempered at 240 °C for 15 hours.

The samples were one previously oxidised pDCPD polyHIPE with 80% porosity and a specimen of H39. The pDVB sample changed colour to light brown, and the pDCPD sample which already was brown in colour acquired a darker hue upon soaking and drying. Both samples became even darker during the tempering process.

Subsequently, a part of each sample was removed, and analysed with XRD. The results are given below in Figure 41.
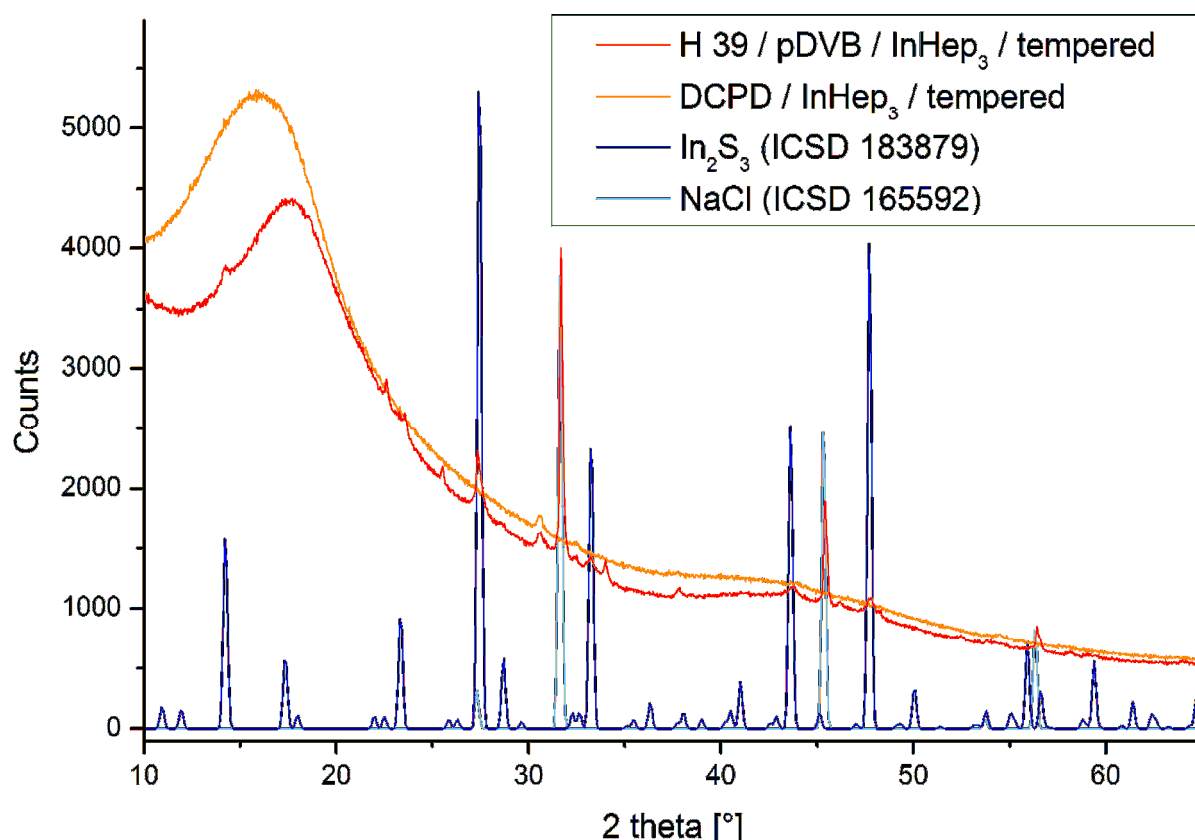
Figure 41: XRD spectrum of polyHIPEs soaked with acetone/InHep₃ solution

The recorded XRD spectrum suggests a successful incorporation of xanthate into the pDVB polyHIPE with subsequent sulphide formation, but no such thing in the pDCPD specimen as no In_2S_3 signal can be discerned. As expected, the pDVB sample gives also a strong NaCl signal. Additionally, EDX analysis was performed on the samples, whose results are displayed in Table 12.

Table 12: EDX analysis of soaked samples after tempering

Sample:	pDCPD		H39 / pDVB	
Element	**Weight %**	**Atomic %**	**Weight %**	**Atomic %**
C	77.70	83.12	89.82	94.15
O	20.81	16.71	4.63	3.64
Na			2.16	1.18
Cl			2.65	0.94
In	1.50	0.17	0.73	0.08
Total	100	100	100	100

When analysed by EDX, both samples give discernible indium signals, although not as strong as expected, thus minimising the advantage of this particular method.

5. Summary and outlook

An indium xanthate – pDVB model system has been developed and tested for the possibility of sulphide incorporation into polyHIPEs. It has been shown that it is indeed possible to incorporate metal xanthates into pDVB through in-situ polymerisation of xanthate solutions, and convert them to the corresponding metal xanthates through thermal treatment. However, due to low xanthate solubility in the monomer, the sulphide content of the polymers remains very low, making the produced specimens unsuitable for production of carbide-carbon composite cathodes.

Another means of xanthate incorporation did give certain results, but in this case the sulphide concentration also remained too low to be applied for cathode production.

Due to the low amounts of incorporated metal, it was in both cases not possible to investigate whether or not metal carbides were formed.

Although the given negative results seem disappointing, the xanthate approach still retains potential. The metal xanthates tested have the disadvantage of the central atom being not fully enclosed by the xanthate moieties, reducing the lipophilic character of the molecule and therefore also reducing its solubility in the monomer. This inconvenience can be overcome by using a compound that fully encloses the metal atom within its substituents. A most suitable choice is cyclopentadienyl titanium xanthate (cpTiHex$_3$) whose major advantage is that the coordinated cyclopentadienyl ring, which is positioned orthogonally to the cp-Ti bond, and shields the titanium cenral atom from its surroundings. This build will most certainly cause a major increase in solubility, improving the prospect of a suitable cathode material.

In another approach to be tested, the xanthate should be ground into fine powder, and suspended throughout the monomer. Upon polymerisation the particles would be enclosed by the polymer, and could be converted into sulphides by conventional means of tempering. This would give larger sulphide particles after polymerisation, however, the sulphide content could be increased dramatically. According to the results from tempering of pure xanthate powder, mean particle size should not exceed 10 nm. Yet it is unclear if the amounts of gas produced inside the polymer during tempering would result in bursting of the matrix.

6. Experimental

6.1.   Reagents

A list of chemicals can be found in Table 13. All chemicals, solvents and auxiliary materials were commercially purchased from commercial dealers and used without any further purification unless stated otherwise. Commercial sources were abcr GmbH, Alfa Aesar GmbH & Co KG, Fluka Chemie AG, Lactan Chemikalien & Laborgeräte GmbH & Co. KG, Orgentis Chemicals GmbH, and Sigma-Aldrich Co. LLC. M2 catalyst ([1,3-bis(2,4,6-trimethylphenyl)-2-imidazolidinylidene]dichloro(3-phenyl-1H-inden-1-ylidene)(tricyclohexylphosphine)ruthenium(II)) for ring opening metathesis polymerisation (ROMP) was obtained from UMICORE AG & Co. KG

Table 13: Purchased chemicals and solvents

Chemicals	Supplier
Ammonium persulfate	Fluka
Bismuth(III) chloride	SIGMA-ALDRICH
Dibenzoylperoxide	Fluka
Dicyclopentadiene	Fluka
Divinylbenzene (80%)	ALDRICH
M2, [1,3-bis(2,4,6-trimethylphenyl)-2-imidazolidinylidene]dichloro(3-phenyl-1H-inden-1-ylidene)(tricyclohexylphosphine)ruthenium(II)	UMICORE
Potassium hydroxide	SIGMA-ALDRICH
Potassium tert-butoxide	ALDRICH
Sodium chloride	VWR CHEMICALS
Span 80	SIGMA-ALDRICH
Styrene	SIGMA-ALDRICH
Titanium tetrachloride	Fluka

6.2.   Instruments

6.2.1.   SEM

Scanning electron microscopy was performed on a VEGA 3 SB Analytic Scanning Electron Microscope. A tungsten cathode at 10 - 20 kV was used as an electron source. The samples were mounted onto aluminium sample holders with

conductive adhesive carbon tape. To ensure their conductivity and therefore visibility in SEM, polymer samples were sputtered with 100 nm of gold prior to measurement, except for the carbonised specimens, which possessed a high enough conductivity without additional treatment. Sputtering was performed on a Cressington Sputter Coater 108auto.

6.2.2. EDX

EDX analysis was carried out with an INCAx-act Analytical Silicon Drift Detector with PentaFET® Precision from Oxford Instruments which was mounted on the SEM. The emission standards were as follows: C ($CaCO_3$), O (SiO_2), Na (Albite), S (FeS_2), C, (KCl), In (InAs)

6.2.3. Tube Furnace

Heat treatment below 500 °C was performed on a tube furnace model Nabertherm R50/500/12 with a heated length of 500 mm, and a custom glass tube which can be seen in Figure 44. The tube was of 40 mm in diameter and had ground glass joints of NS 40/38 on the inlet side and NS 14/23 on the outlet side. The length of the pipe that was inside the furnace was 650 mm. The inlet side was closed with a glass valve which was connected to a silicone hose. The outlet side was closed with a gas bubbler filled with silicon oil to ensure a

Figure 42: Schematic cross-section of glass tube to illustrate how the samples were positioned

separation from the atmosphere. Nitrogen and pressurised air were taken from the university's gas lines, reduced by a pressure regulator to 1,2 bar and adjusted via a KROHNE DK800 R flowmeter which was connected to the previously described glass tube with a silicone hose.

The samples were placed inside the tube on a vessel made from folded aluminium foil with a thickness of 30 µm as shown in Figure 42. The aluminum foil was folded in a manner that was supposed to minimize the area of contact between foil and sample, but hold it in a vertical position during tube insertion. To inhibit
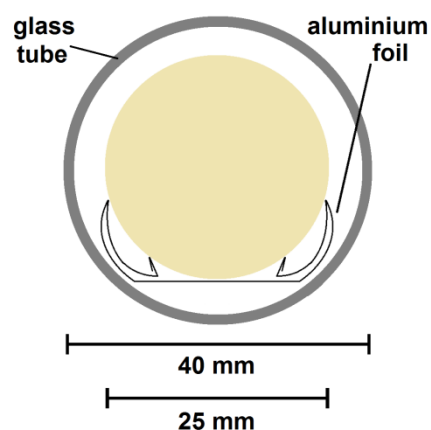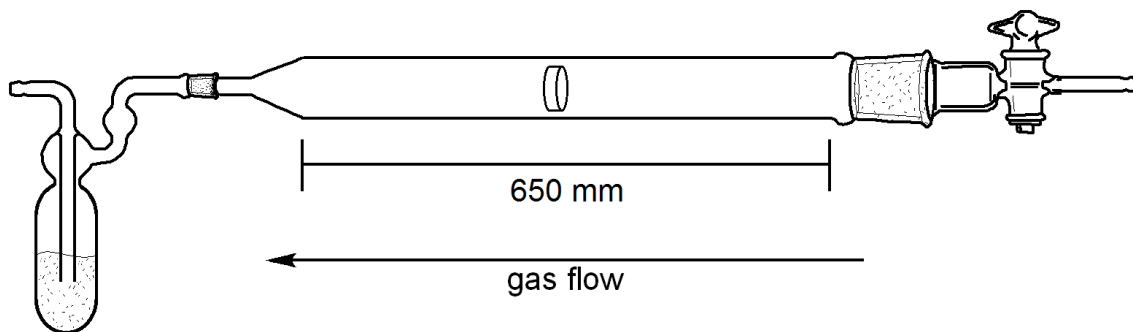
45

convection of cold gas from the ends of the tube towards the inside, two balls made from aluminium foil were placed inside the tube before and after the vessel.

Figure 44: Glass tube, inlet valve and bubbler inside the tube furnace

Figure 43: Samples placed in glass tube with balls of aluminium foil placed before and after the vessel

Carbonisation of the samples was performed by Katharina Gruber on a Carbolite TZF 15/610 High Temperature 3 Zone Tube Furnace with a heated length of 610 mm and a tube diameter of 90 mm under argon flow.

6.2.4. Compression-modulus

Compression moduli were acquired on a Shimadzu Autograph AGS-X with a force measuring range of 1 N - 10 kN. The foam samples were loaded at a speed of 1 mm min^{-1} with 100 measurements per second
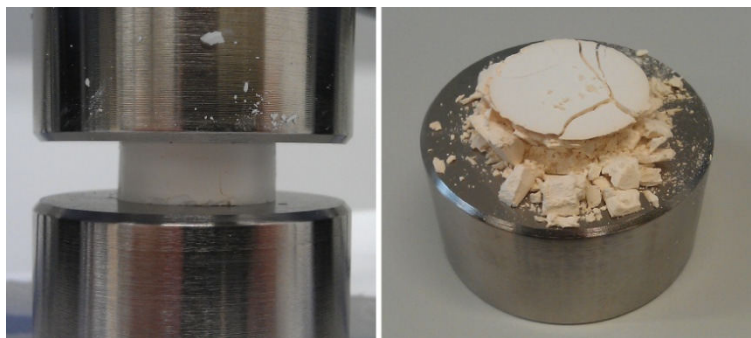

Figure 45: left frame: crack in a polyHIPE during testing; right frame: polyHIPE after 30% compression

until the displacement was 30% of the examined sample's height. The Young's modulus was determined from the first derivation of the initial linear slope of the stress/strain plot with a sliding average smoothing algorithm with 51 points. The crush strength was defined as the maximum strength at the end of the elastic region.

6.2.5. XRD

X-ray powder diffraction profiles were measured with a Siemens D-5005 powder diffractometer with Bragg-Brentano θ/θ geometry, operated at 40 kV and 30 mA, using Cu Kα radiation, a graphite monochromator, a scintillation counter The step width was 0.02° with constant counting times of 20 s/step. Samples were ground into fine powder using a porcelain mortar and pestle prior to measurement.

6.2.6. FTIR

Fourier transformed infrared spectrometry was performed on a Perkin Elmer Spectrum One FT-IR Spectrometer. All spectra were recorded in a range from 450 to 4000 cm^{-1} in attenuated total reflectance (ATR) mode with 10 scans per spectrum and a resolution of 4 cm^{-1}.

6.2.7. NMR

NMR measurements were performed on a Bruker Ultrashield 300. The Spectra were recorded from whether D_2O or $CDCl_3$ solvents, depending on the analyte's solubility. ^{1}H-NMR spectra were obtained at 300 MHz and ^{13}C-NMR spectra at 75MHz. ^{1}H-NMR chemical shifts are reported in parts per million (ppm) relative to the

signals of D_2O or $CDCl_3$ at 4.63 ppm and 7.24 ppm accordingly. ^{13}C-NMR shifts are referenced to the signals of $CDCl_3$ at 77.230 ppm.

6.2.8. STA

The STA measurements were performed by Josefine Hobisch on a Netzsch Jupiter STA 449C Thermoanalysator in Al_2O_3 crucibles. Measurements were performed at a heating rate of 10 °C min^{-1}, in helium or nitrogen atmosphere as reported in the experiment descriptions.

6.3. Preparation of Metal Xanthates

Xanthates were prepared based on procedures described by Alex Schenk[19] and Verena Kaltenhauser.[90]

6.3.1. Potassium-O-3,3-dimethylbutan-2-yl dithiocarbonate - KHex

Potassium tert-butoxide was dissolved in THF and cooled to 0 °C under a nitrogen flow using an ice bath. Afterwards the alcohol was added slowly while stirring and after several minutes carbon disulphide was added dropwise through a dropping funnel. The reaction mixture was then stirred for at least 5 hours before the solution was diluted with diethyl ether. The resulting solid was dried in vacuum before it was dissolved again in acetone to remove insoluble side products. The acetone phase was concentrated by rotary evaporation before the product was precipitated through addition of diethyl ether. The product was then separated by filtration and dried in vacuum. The amounts of chemicals used are given in Table 14.

Table 14: Preparation of potassium-O-3,3-dimethylbutan-2-yl dithiocarbonate - KHex

Reagent	MW [g/mol]	Mass [g]	Volume [mL]	Equivalents	THF volume [mL]
tBuOK	112.22	6.9217		1.0	80
HexOH	102.18	7.5410		1.1	
CS$_2$	76.14	5.0318		1.1	
THF			80		

Yield: 9.9652 g (74.52%)

^{1}H-NMR (acetone-D6, [ppm]) 5.43-5.36 (q), 1.11-1.09 (d), 0.91 (s)

^{13}C-NMR (acetone-D6) 233.65, 84.36, 35.32, 26.46, 14.77

IR: 2963, 2870, 1474, 1456, 1393, 1377, 1363, 1223, 1208, 1133, 1101, 1085, 1066, 1030

6.3.2. Bismuth-O-3,3-dimethylbutan-2-yl dithiocarbonate - BiHex$_3$

Bismuth (III)-chloride was dissolved in 50 mL H_2O in a three-necked round-bottom flask. A white precipitate that consisted of BiOCl was rapidly formed and stuck to the vessel. The potassium xanthate was dissolved in 20 mL H_2O and added dropwise to the solution under vigorous stirring. A brown precipitate was slowly formed. The reaction was allowed to stir over night, after which 20 mL DCM were added. The reaction vessel was shaked vigorously and the resulting two phased mixture was transferred into a separating funnel. The yellow organic phase was separated from the aqueous phase which was then extracted two additional times with 20 mL DCM. All three organic phases were collected, fused and then reduced by rotary evaporation. The resulting solution was then left at -20 °C for several hours during which elongated, 2-3 mm long crystals were formed. The amounts of chemicals used are given in Table 15.

Table 15: Preparation of bismuth-O-3,3-dimethylbutan-2-yl dithiocarbonate - BiHex$_3$

Reagent	MW [g/mol]	Mass [g]	Volume [mL]	Equivalents	H_2O volume [mL]
BiCl$_3$	315.34	0.8611		1.0	50
KHex	216.40	1.7139		3.1	
DCM			40		

Yield: 1.7395 g, (91.16 %)

^{1}H NMR (CDCl$_3$, [ppm]) 5.43-5.36 (dd), 1.11-1.09 (d), 0.91 (s)

^{13}C NMR (CDCl$_3$, [ppm]) 233.65, 84.36, 35.32, 26.46, 14.77

IR: 2965, 2873, 1479, 1397, 1378, 1366, 1339, 1235, 1211, 1113, 1074, 1049, 1018, 876

6.3.3. Bismuth-O-3,3-dimethylpentan-2-yl dithiocarbonate - BiHep$_3$

BiHep$_3$ was prepared in the same manner as BiHex$_3$. The amounts of chemicals used are given in Table 16.

Table 16: Preparation of bismuth-O-3,3-dimethylpentan-2-yl dithiocarbonate - BiHep$_3$

Reagent	MW [g/mol]	Mass [g]	Volume [mL]	Equivalents	H$_2$O volume [mL]
BiCl$_3$	315.34	0.8513		1.0	50
KHep	230.43	1.9910		3.2	
DCM			40		

Yield: 1,6482 g, (82,41%)

^{1}H NMR (CDCl$_3$, [ppm]) 5,64-5,59 (dd), 1,68-1,46 (m), 0,93-0,89 (s)

^{13}C NMR (CDCl$_3$, [ppm]) 227.08, 96.40, 35.90, 26.11, 23.19, 11.07

FTIR [cm^{-1}] 2969, 2875, 1478, 1467, 1397, 1367, 1340, 1232, 1211, 1198, 1128, 1081, 1052, 1026, 902

6.3.4. Titanium-O-3,3-dimethylpentan-2-yl dithiocarbonate - TiHep$_4$

The Reaction was performed under strictly anhydrous conditions under N$_2$ atmosphere.

Titanium (IV)-chloride was dissolved in 50 mL THF. The potassium xanthate was dissolved in 20 mL THF and added dropwise to the solution under vigorous stirring. A bright orange solution resulted shortly after addition of the first drops, which then faded to a bleak yellow colour with a white precipitate. The reaction was allowed to stir for about 5 hours. The Solution was filtered using a Schlenk-frit which quickly clogged with the product, which was not analysable afterwards.

The desired titanium xanthate could not be isolated. This speaks for the nonionic, but coordinative nature of the bond. The amounts of chemicals used are given in Table 17.

Table 17: Preparation of titanium-O-3,3-dimethylpentan-2-yl dithiocarbonate - TiHep$_4$

Reagent	MW [g/mol]	Mass [g]	Volume [mL]	Equivalents	THF volume [mL]
TiCl$_4$	189.68	0.2565		1.0	50
KHep	230.43	1.2770		4.1	20
THF			70		

Yield: 0 g (0%)

6.4.   Preparation of polyHIPEs

PolyHIPEs were prepared based on instructions from literature, but were adapted to the task at hand. All components were measured gravimetrically, except for water, which was measured volumetrically.

Surfactant, monomers, xanthates, and DBP were mixed in the three-necked round-bottom flask, in which the emulsion was to be prepared, and stirred with a mechanical stirrer at 500 rpm until complete dissolution of DBP after five minutes. NaCl, APS and water were mixed in a 50 mL PE test tube with a blue screw cap, then transferred to a dropping funnel, and added to the continuous phase during 10 minutes, while stirred at 500 rpm. After complete addition of the aqueous phase stirring was continued for further 30 min. After switching off and removing the stirrer, the emulsion was quickly transferred into 20 mL glass vials with screw caps which served as moulds and placed in an oven for approximately 24 h. The resulting pHIPEs were retrieved by carefully breaking the vials without damaging the pHIPEs, and rinsed with deionised water to remove glass shards. They were then dried in an oven at 80 °C for another 24 h.

Detailed amounts of the polyHIPE preparation parameters can be seen in Tables 18 to 20 on the following pages

6.5.   Heat treatment of polyHIPEs

The heat treatment was performed in the tube furnace described in Chapter 6.2.3 Tube Furnace.

Detailed results can be seen in Table 21 on Page 56.

The gas bubbler at the end of the glass furnace tube produced certain variations in flow rate. Every time a bubble left the end of the glass tube inside the silicon oil the

gas flow would shortly go up, and then decrease to the previous amount when the bubble disconnected from the tube, thus causing a minimal oscillation in pressure which in turn caused an oscillation in gas flow. Since the oscillations were constant and uniform, the lower and upper values of gas flow rates are given in the corresponding column of Table 21.

Table 18: Preparation of polyHIPEs

Sample #	Monomer mass [g]	DBP mass [g]	APS mass [g]	Surfactant mass [g]	NaCl mass [g]
H01	6.4330	0.2461	-	0.7701	0.3751
H02	3.2165	0.1243	-	0.3890	0.1883
H03	3.2165	0.1212	-	0.3813	-
H04	6.4330	0.2460	-	0.7742	-
H05	7.3176	0.0815	-	0.8890	-
H06	7.3225	0.0815	-	0.8871	0.4328
H07	7.3240	0.0417	0.1402	0.8888	-
H08	7.3419	0.0409	0.1396	0.8871	0.4330
H09	7.3274	0.0845	-	0.8929	-
H10	7.3270	0.0839	-	0.8905	0.4344
H11	7.3145	0.0412	0.1422	0.8902	-
H12	7.3254	0.0405	0.1424	0.8890	0.4355
H13	3.6593	0.0205	0.0702	0.4466	-
H14	3.6649	0.0212	0.0706	0.5576	0.2160
H15	3.6966	0.0207	0.0708	0.4517	0.2188
H16	3.6725	0.0205	0.0674	0.4435	0.2160
H17	0.9194	0.0132	0.3210	0.2019	0.4306
H18	1.5311	0.0071	0.0305	0.3047	0.2106
H19	2.4339	0.0137	0.0497	0.4843	0.2224
H20	3.4464	0.0178	0.0706	0.6995	0.2520
H21	1.5245	0.0068	0.3020	0.3028	0.2346
H22	2.4245	0.0140	0.0494	0.4840	0.2261
H23	3.2352	0.0325	-	0.3261	0.3007
H24	4.5901	0.0461	-	0.4587	2.0017
H25	4.5872	0.0472	-	0.4570	1.9974
H26	3.2540	-	0.3023	0.3335	0.3009
H27	4.5837	-	0.2991	0.4582	0.3009
H28	4.5897	0.0254	0.0996	0.4510	0.3037
H29	4.5943	0.0251	0.1025	0.4588	0.3013
H30	4.5909	0.0239	0.1045	0.4561	0.3001
H31	4.5862	0.0232	0.1016	0.4560	0.3054
H32	4.5801	0.0229	0.1035	0.4612	0.3013
H33	4.5935	0.0245	0.1003	0.4582	0.3023
H34	4.5951	0.0239	0.1004	0.4606	0.3017
H35	4.5887	0.0242	0.1033	0.4604	0.3023
H36	4.5882	0.0234	0.1024	0.4676	0.2983
H37	4.5902	0.0240	0.1021	0.4649	0.3003
H38	9.1912	0.0457	0.2019	0.9186	0.6008
H39	9.2018	0.0470	0.2020	0.9152	0.6004
H40	9.2960	0.0461	0.2037	0.9283	0.6086
H41	9.2641	0.0468	0.2466	0.9260	0.7225

Table 19: Preparation of polyHIPEs, continuation

Sample #	Xanthate type	Xanthate mass [g]	Surfactant amount [m%] of.Mon.	NaCl amount [m%] of H_2O	Theoretical porosity [%]
H01	CdHep$_2$	0.284	11.97	1.44	78.79
H02	-	-	12.09	1.45	78.79
H03	-	-	11.85		78.79
H04	InHep$_3$	0.9580	12.03		78.79
H05	-	-	12.15		79.03
H06	-	-	12.11	1.44	79.01
H07	-	-	12.14		79.01
H08	-	-	12.08	1.44	78.97
H09	-	-	12.19		79.01
H10	-	-	12.15	1.45	79.01
H11	-	-	12.17		79.03
H12	-	-	12.14	1.45	79.01
H13	InHep$_3$	1.5314	12.20		79.03
H14	InHep$_3$	1.5312	15.21	1.44	78.99
H15	-	-	12.22	1.46	78.78
H16	-	-	12.08	1.44	78.95
H17	-	-	21.96	2.15	95.24
H18	-	-	19.90	1.40	89.98
H19	-	-	19.90	1.48	84.99
H20	-	-	20.30	1.68	80.00
H21	-	-	19.86	1.56	90.04
H22	-	-	19.96	1.51	85.03
H23	-	-	10.08	1.50	85.03
H24			9.99	10.01	80.03
H25			9.96	9.99	80.03
H26			10.25	1.50	84.96
H27			10.00	1.50	80.03
H28			9.83	1.52	80.03
H29	BiHex$_3$	0.2987	9.99	1.51	80.00
H30	GaHex$_3$	0.5050	9.93	1.50	80.00
H31	InHex$_3$	0.4590	9.94	1.53	80.03
H32	CdHep$_2$	0.2713	10.07	1.51	80.06
H33	GaHep$_3$	0.0681	9.97	1.51	80.00
H34	InHep$_3$	0.8265	10.02	1.51	80.00
H35	MnHepPhen	0.0287	10.03	1.51	80.03
H36	SbHep$_3$	0.1788	10.19	1.49	80.03
H37	ZnHep$_2$	0.0992	10.13	1.50	80.03
H38	-	-	9.99	1.50	80.00
H39	-	-	9.95	1.50	79.98
H40	InHep$_3$	0.9388	9.99	1.27	82.59
H41	-	-	10.00	1.51	82.64

Table 20: Preparation of polyHIPEs, continuation

Sample #	Monomer type	Surfactant type	Flask volume [mL]	Curing-temperature [℃]	Curing Time [h]	theoretical density [g/cm^3]
H01	DVB	Span 80	100	60 ℃	24	0.23
H02	DVB	Span 80	100	60 ℃	24	0.22
H03	DVB	Span 80	100	60 ℃	24	0.22
H04	DVB	Span 80	100	60 ℃	24	0.25
H05	DVB	Span 80	100	80 ℃	6	0.21
H06	DVB	Span 80	100	80 ℃	6	0.21
H07	DVB	Span 80	100	80 ℃	5	0.21
H08	DVB	Span 80	100	80 ℃	6	0.21
H09	DVB+Styrene	Span 80	100	80 ℃	5	0.21
H10	DVB+Styrene	Span 80	100	80 ℃	5	0.21
H11	DVB+Styrene	Span 80	100	80 ℃	5	0.21
H12	DVB+Styrene	Span 80	100	80 ℃	5	0.21
H13	DVB	Span 80	100	80 ℃	16	0.29
H14	DVB	Span 80	100	80 ℃	24	0.30
H15	DVB+Styrene	Span 80	100	85 ℃	17	0.21
H16	DVB	Span 80	100	80 ℃	23	0.21
H17	DVB	Span 80	100	83 ℃	23	0.05
H18	DVB	Span 80	100	83 ℃	17	0.11
H19	DVB	Span 80	100	83 ℃	16	0.16
H20	DVB	Span 80	100	83 ℃	18	0.21
H21	DVB	Span 80	100	83 ℃	17	0.11
H22	DVB	Span 80	100	83 ℃	16	0.16
H23	DVB	Span 80	100	83 ℃	17	0.15
H24	DVB	Span 80	100	80 ℃	17	0.20
H25	DVB	Span 80	100	80 ℃	29	0.20
H26	DVB	Span 80	100	80 ℃	25	0.15
H27	DVB	Span 80	100	80 ℃	22	0.20
H28	DVB	Span 80	100	80 ℃	24	0.20
H29	DVB	Span 80	100	80 ℃	21	0.21
H30	DVB	Span 80	100	80 ℃	21	0.22
H31	DVB	Span 80	100	80 ℃	27	0.22
H32	DVB	Span 80	100	80 ℃	22	0.21
H33	DVB	Span 80	100	80 ℃	27	0.20
H34	DVB	Span 80	100	80 ℃	23	0.23
H35	DVB	Span 80	100	80 ℃	22	0.20
H36	DVB	Span 80	100	80 ℃	22	0.21
H37	DVB	Span 80	100	80 ℃	25	0.20
H38	DVB	Span 80	250	80 ℃	24	0.20
H39	DVB	Span 80	250	80 ℃	23	0.20
H40	DVB	Span 80	250	80 ℃	24	0.19
H41	DVB	Span 80	250	80 ℃	29	0.17

Table 21: Detailed description of polyHIPE heat treatment

Sample #	Heat-up time $t_{RT \to T_1}$ [hh:mm]	Dwell temp. T_1 [℃]	Dwell time t_{dwell} [hh:mm]	Gas flow rate [l/min]	Gas	Raw mass m_0 [g]	Tempered mass m_t [g]	Mass difference [%]	Oxidised mass m_O [g]	Mass difference [%]	Carbonised mass m_C [g]	Mass difference [%]
H38 I	00:15	200	02:00	1.5-2.0	O_2				0,09283			
H38 I	01:20	430	01:30	1.5-2.0	N_2							
H38 I	03:40	900	02:00	?	Ar						0.0523	-43.66%
H39_I	02:00	140	02:00	1.5-2.0	O_2	1.19147			1.18222			
H40	02:00	200	02:00	2.5-3.0	N_2							
H39_II	02:00	120	03:00	2.5-3.0	O_2	1.22473			1.22765			
H39_III	02:00	100	05:00	2.5-3.0	O_2	0.97381			0.99305			
H39_IV	02:00	100	05:00	2.5-3.0	O_2	0.54614						
H39_IV	02:00	110	03:00	2.5-3.0	O_2				0.55544	+1.70%		
H39_V	02:00	110	03:00	2.5-3.0	O_2	0.97680			0.99747			
H40_I	02:00	110	05:00	2.5-3.0	O_2	0.88203	0.85583	-2.97%				
H40_II	02:00	110	05:00	2.5-3.0	O_2				0.85929	+0.14%		
H40_II	01:00	200	00:00	2.5-3.0	N_2	0.88647	0.85809	-3.20%				
H40_II	05:00	500	04:00	2.5-3.0	N_2							
H40_II	03:40	900	02:00	?	Ar						0.2213	-74.25%
H40_III	02:00	230	03:00	2.5-3.0	N_2	0.88477	0.84823	-4.13%				
H40_IV	03:00	240	11:00	1.5-2.0	N_2	0.87548	0.82790	-5.43%				
H40_V	03:00	240	15:00	2.0-5.0	N_2	0.89330	0.85245	-4.57%				
H40_VI	03:00	240	15:00	2.0-5.0	N_2	0.88969	0.84697	-4.80%				
H40_VI	02:00	110	08:00	1.0-2.0	O_2				0.84726	+0.03%		
H40_VII	03:00	240	15:00	2.0-5.0	N_2	0.87151	0.82725	-5.08%				
H40_VII	02:00	110	08:00	1.0-2.0	O_2				0.82747	+0.03%		
H40_VIII	03:00	240	15:00	2.0-5.0	N_2	0.88954	0.84127	-5.43%				
H40_VIII	02:00	110	08:00	1.0-2.0	O_2				0.84152	+0.03%		
H29_III	03:00	240	15:00	1.0-2.0	N_2	1.05811	0.99515	-5.95%				

7. Appendix

7.1. Abbreviations

APS	ammonium persulfate
BET	Brunauer Emmet Teller
DBP	dibenzoylperoxide
DCM	dichloromethane
DCPD	dicyclopentadiene
DSC	differential scanning calorymetry
EDX	enerdy dispersive X-ray spectroscopy
HIPE	high internal phase emulsion
HLB	hydrophilic-lipophilic balance
ICSD	Inorganic Crystal Structure Database
IUPAC	International Union of Pure and Applied Chemistry
NMR	nuclear magnetic resonance spectroscopy
pDCPD	polydicyclopentadiene
polyHIPE	polymerised high internal phase emulsion
PS	polystyrene
RT	room temperature
SEM	scanning electron microscopy
STA	simultaneous thermal analysis
TGA	thermogravimetrical analysis
XRD	X-ray diffractometry
$BiHep_3$	bismuth(III) O-2,2-dimethylpentan-3-yl dithiocarbonate
$BiHex_3$	bismuth(III) O-2,2-dimethylbutan-3-yl dithiocarbonate
$CdHep_2$	cadmium(II) O-2,2-dimethylpentan-3-yl dithiocarbonate
CuHep	copper(I) O-2,2-dimethylpentan-3-yl dithiocarbonate
$GaHep_3$	gallium(III) O-2,2-dimethylpentan-3-yl dithiocarbonate
$GaHex_3$	gallium(III) O-2,2-dimethylbutan-3-yl dithiocarbonate
$InHep_3$	indium(III) O-2,2-dimethylpentan-3-yl dithiocarbonate
$InHex_3$	indium(III) O-2,2-dimethylbutan-3-yl dithiocarbonate

MnHepPhen$_3$ manganese(II) 1,10-phenanthroline O-2,2-dimethylpentan-3-yl dithiocarbonate

NiHep$_2$ nickel(II) O-2,2-dimethylpentan-3-yl dithiocarbonate

PbHep$_2$ lead(II) O-2,2-dimethylpentan-3-yl dithiocarbonate

SbHep$_3$ antimony O-2,2-dimethylpentan-3-yl dithiocarbonate

TiHep$_4$ titanium(IV) O-2,2-dimethylpentan-3-yl dithiocarbonate

ZnEt$_2$ zinc O-ethyl dithiocarbonate

ZnHep$_2$ zinc O-2,2-dimethylpentan-3-yl dithiocarbonate

ZnHex$_2$ zinc O-2,2-dimethylbutan-3-yl dithiocarbonate

7.2. List of figures

7.3.   List of tables

7.4. References

1. Yamamoto, O. *The Lithium Air Battery: Fundamentals*. (Springer Science+Business Media New York, 2014). doi:10.1007/978-1-4899-8062-5

2. Abraham, K. . M., Jiang, Z. & Soc, J. E. A Polymer Electrolyte – Based Rechargeable Lithium / Oxygen Battery. **143,** 1–5 (1996).

3. Girishkumar, G., McCloskey, B., Luntz, a. C., Swanson, S. & Wilcke, W. Lithium-air battery: Promise and challenges. *J. Phys. Chem. Lett.* **1,** 2193–2203 (2010).

4. Bruce, P. G., Freunberger, S. a., Hardwick, L. J. & Tarascon, J.-M. Li–O2 and Li–S batteries with high energy storage. *Nat. Mater.* **11,** 172–172 (2011).

5. Kumar, B. *et al.* A Solid-State, Rechargeable, Long Cycle Life Lithium–Air Battery. *J. Electrochem. Soc.* **157,** A50 (2010).

6. Kwabi, D. G. *et al.* Materials challenges in rechargeable lithium-air batteries. *MRS Bull.* **39,** 443–452 (2014).

7. Cameron, N. R., Krajnc, P. & Silverstein, M. S. *Porous polymers*. (John Wiley & Sons, Inc., 2011).

8. Roy, K.-M. in *Ullmann's Encyclopedia of Industrial Chemistry* (Wiley-VCH Verlag GmbH & Co. KGaA, 2000). doi:10.1002/14356007.a28_423

9. Rao, R. S. *Xanthates and Related Compounds*. (Marcel Dekker, 1971).

10. Zeise, W. C. Vorläufige Anzeige einer neuen Classe von Schwefelverbindungen. *J. Chem. Phys* **35,** 173 (1822).

11. Tschugaeff, L. Ueber eine neue Methode zur Darstellung ungesättigter Kohlenwasserstoffe. *Berichte der Dtsch. Chem. Gesellschaft* **32,** 3332–3335 (1899).

12. Hebert, A. M. Sur la décomposition pyrogénée des xanthates métalliques. *Bull. la Société Chim. Fr. Mémoires* **9,** 523–532 (1911).

13. DePuy, C. H. & King, R. W. Pyrolytic Cis Eliminations. *Chem. Rev.* **60,** 431 (1960).

14. Ottakam Thotiyl, M. M. *et al.* A stable cathode for the aprotic Li-O2 battery. *Nat. Mater.* **12,** 1050–6 (2013).

15. Tulhoff, H. in *Ullmann's Encyclopedia of Industrial Chemistry* (Wiley-VCH Verlag GmbH & Co. KGaA, 2000). doi:10.1002/14356007.a05_061

16. Tabor, D. *The Hardness of Materials*. (Oxford University Press Inc., 2000).

17. Kovačič, S. unpublished results.

18. Gomez, I. . *An. la Soc. Española Física y Química* **14,** 91–102 (1916).

19. Schenk, A. Novel metal-xanthates for preparation of metal sulphides for photovoltaic applications. (Graz University of Technology, 2011).

20. González-Roura, A., Casas, J. & Llebaria, A. Synthesis and phospholipase C inhibitory activity of D609 diastereomers. *Lipids* **37,** 401–406 (2002).

21. Pradhan, N., Katz, B. & Efrima, S. Synthesis of High-Quality Metal Sulfide Nanoparticles from Alkyl Xanthate Single Precursors in Alkylamine Solvents. *J. Phys. Chem. B* **107,** 13843–13854 (2003).

22. Pradhan, N. & Efrima, S. Single-precursor, one-pot versatile synthesis under near ambient conditions of tunable, single and dual band fluorescing metal sulfide nanoparticles. *J. Am. Chem. Soc.* **125,** 2050–2051 (2003).

23. Nair, P. S., Radhakrishnan, T., Revaprasadu, N., Kolawole, G. a & O'Brien, P. A single-source route to CdS nanorods. *Chem. Commun. (Camb).* 564–565 (2002). doi:10.1039/b200434h

24. Trindade, T., O'Brien, P., Zhang, X. & Motevalli, M. Synthesis of PbS nanocrystallites using a novel single molecule precursors approach: X-ray single-crystal structure of Pb(S2CNEtPri)2. *J. Mater. Chem.* **7,** 1011–1016 (1997).

25. Ludolph, B. & Malik, M. a. Novel single molecule precursor routes for the direct synthesis of highly monodispersed quantum dots of cadmium or zinc sulfide or selenide. *Chem. Commun.* **3,** 1849–1850 (1998).

26. Lazell, M. & O'Brien, P. A novel single source precursor route to self capping CdS quantum dots. *Chem. Commun.* 2041–2042 (1999). doi:10.1039/a906160f

27. Green, M. & O'Brien, P. Recent advances in the preparation of semiconductors as isolated nanometric particles: new routes to quantum dots. *Chem. Commun.* 2235–2241 (1999). doi:10.1039/a904202d

28. Fischereder, A. Synthesis and characterization of metal sulfides for photovoltaic applications. (Graz University of Technology, 2011).

29. Publications, B. S. in *IUPAC Compendium of Chemical Terminology* (eds. McNaught, A. D. & Wilkinson, A.) (Blackwell Scientific Publications, 2005). doi:10.1351/goldbook.M03853

30. Rouquerol, J., Rouquerol, F., Llewellyn, P., Maurin, G. & Sing, K. *Adsorption by Powders and Porous Solids: Principles, Methodology and Applications.* (Academic Press, Elsevier Ltd., 2014).

31. Lissant, K. J. The Geometry of High-Internal-Phase-Ratio Emulsions. **m,** 462–468 (1966).

32.   Kepleri, J. *Strena seu de nive sexangula*. (1611).

33.   Cameron, N. R., Sherrington, D. C., Albiston, L. & Gregory, D. P. Study of the formation of the open-cellular morphology of poly(styrene/divinylbenzene) polyHIPE materials by cryo-SEM. *Colloid Polym. Sci.* **274,** 592–595 (1996).

34.   Griffin, W. Classification of surface-active agents by' HLB'. *J Soc Cosmet. Chem.* 311–326 (1946). at <http://ci.nii.ac.jp/naid/10004943329/>

35.   Griffin. HLB non ionic surfactants. (1954).

36.   Lissant, K. J. Geometry of emulsions. *J. Soc. Cosmet. Chem.* **21,** 141–154 (1970).

37.   Mannheimer, R. J. Anomalous rheological characteristics of a high-internal-phase-ratio emulsion. *J. Colloid Interface Sci.* **40,** 370–382 (1972).

38.   Pons, R., Solans, C., Stebé, M. J., Erra, P. & Ravey, J. C. Stability and rheological properties of gel emulsions. *Prog. Colloid Polym. Sci.* **89,** 110–113 (1992).

39.   Kizling, J. & Kronberg, B. On the formation and stability of concentrated water-in-oil emuslions, aphrons. *Colloids and Surfaces* **50,** 131–140 (1990).

40.   Kunieda, H., Evans, D. F., Solans, C. & Yoshida, M. The Structure of Gel-Emulsions in a Water / Nonionic Surfactant / Oil System. **47,** 35–43 (1990).

41.   Kunieda, H., Yano, N. & Solans, C. The formation of gel-emulsions in a water-nonionic surfactant-oil system. *Colloids and Surfaces* **24,** 225–237 (1987).

42.   Kunieda, H., Yano, N. & Solans, C. The Stability of Gel-Emulsions in a Water/Non-ionic Surfactant/Oil System. **36,** 313–322 (1989).

43.   Livshin, S. & Silverstein, M. S. Cross-linker flexibility in porous crystalline polymers synthesized from long side-chain monomers through emulsion templating. *Soft Matter* **4,** 1630 (2008).

44.   Barby, D. & Haq, Z. Low density porous cross-linked polymeric materials and their preparation. (1986). at <http://www.google.com/patents/EP0060138B1?cl=en:Method>

45.   Williams, J. M. & Wrobleski, D. a. Spatial Distribution of the Phases in Water-in-Oil Cross-Linked Polystyrene? Emulsions. Open and Closed Microcellular Foams . *Langmuir* **4,** 656–662 (1988).

46.   Schwab, M. G. *et al.* High surface area polyHIPEs with hierarchical pore system. *Soft Matter* **5,** 1055 (2009).

47.   in *IUPAC Compendium of Chemical Terminology* 2315 (2005). doi:10.1351/goldbook.C00840

48. Edwards, C. J. C., Hitchen, D. A. & Sharples, M. Porous carbon structures and methods for their preparation. (1988). at <https://www.google.com/patents/US4775655>

49. Silverstein, M. S. PolyHIPEs: Recent advances in emulsion-templated porous polymers. *Prog. Polym. Sci.* **39,** 199–234 (2014).

50. Wang, D., Smith, N. L. & Budd, P. M. Polymerization and carbonization of high internal phase emulsions. *Polym. Int.* **54,** 297–303 (2005).

51. Silverstein, M. S. Emulsion-templated porous polymers: A retrospective perspective. *Polym. (United Kingdom)* **55,** 304–320 (2014).

52. Cohen, N. & Silverstein, M. S. Synthesis of emulsion-templated porous polyacrylonitrile and its pyrolysis to porous carbon monoliths. *Polymer (Guildf).* **52,** 282–287 (2011).

53. Even, W. R. & Gregory, D. P. Emulsion-derived foams: preparation, properties, and application. *MRS Bull.* **19,** 29–33 (1994).

54. Kovačič, S., Krajnc, P. & Slugovc, C. Inherently reactive polyHIPE material from dicyclopentadiene. *Chem. Commun. (Camb).* **46,** 7504–7506 (2010).

55. Fitzer, E., Frohs, W. & Heine, M. Optimization of stabilization and carbonization treatment of PAN fibres and structural characterization of the resulting carbon fibres. *Carbon* **24,** 387–395 (1986).

56. Bashir, Z. A critical review of the stabilisation of polyacrylonitrile. *Carbon* **29,** 1081–1090 (1991).

57. Davidson, T. a, Wagener, K. B. & Priddy, D. B. Polymerization of Dicyclopentadiene: A Tale of Two Mechanisms. *Macromolecules* **29,** 786–788 (1996).

58. Davidson, T. a. & Wagener, K. B. The polymerization of dicyclopentadiene: An investigation of mechanism. *J. Mol. Catal. A Chem.* **133,** 67–74 (1998).

59. Mol, J. C. Industrial applications of olefin metathesis. *J. Mol. Catal. A Chem.* **213,** 39–45 (2004).

60. Kaplan, N., Peled, G. & Bak, N. Improved ballistic resistant composite articles with polydicyclopentadiene (pdcpd). (2011). at <http://www.google.com/patents/WO2011039737A1?cl=en>

61. Sherman, L. M. Poly-DCPD RIM Shifts into Higher Gear. (2002). at <http://www.ptonline.com/articles/poly-dcpd-rim-shifts-into-higher-gear>

62. Osborne Industries, I. pDCPD Molding: Overview. (2014). at <http://www.osborneindustries.com/dcpd-molding.php>

63. Manley, S. S. *et al.* New insights into the relationship between internal phase level of emulsion templates and gas–liquid permeability of interconnected macroporous polymers. *Soft Matter* **5,** 4780 (2009).

64. Kovačič, S., Matsko, N. B., Jerabek, K., Krajnc, P. & Slugovc, C. On the mechanical properties of HIPE templated macroporous poly(dicyclopentadiene) prepared with low surfactant amounts. *J. Mater. Chem. A* **1,** 487 (2013).

65. Williams, J., Gray, A. & Wilkerson, M. Emulsion stability and rigid foams from styrene or divinylbenzene water-in-oil emulsions. *Langmuir* **6,** 437–444 (1990).

66. Letts, S. A. in *Laser Program Annual Report* (eds. O'Neal, E. M., Murphy, P. W. & Haendler, B. L.) (Lawrence Livermore National Laboratory, 1987). at <https://books.google.at/books?id=IZbvAAAAMAAJ>

67. Bicerano, J., Sammler, R. L., Carriere, C. J. & Seitz, J. T. Correlation between glass transition temperature and chain structure for randomly crosslinked high polymers. *J. Polym. Sci. Part B Polym. Phys.* **34,** 2247–2259 (1996).

68. Alivisatos, a. P. Nanocrystals: Building blocks for modern materials design. *Endeavour* **21,** 56–60 (1997).

69. Mostafa a. El-Sayed. Small Is Different: Shape-,Size-, and Composition-Dependent Properties of Some Colloidal Semiconductor Nanocrystals. *Acc. Chem. Res* **37,** 326 (2004).

70. Ashton, H. C. in *Polymer nanocomposites handbook* (eds. Gupta, R. K. ., Kennel, E. & Kim, K.-J.) 21–44 (CRC Pres, 2010). doi:10.1201/9781420009804-c3

71. Cheng, Z. *Advances in Nanocomposite Technology. Advances in Nanocomposite Technology* (InTech, 2011). doi:10.5772/676

72. Vaia, R. A., Ishii, H. & Giannelis, E. P. Synthesis and Properties of Two-Dimensional Nanostructures by Direct Intercalation of Polymer Melts in Layered Silicates. *Chem. Mater.* **5,** 1694–1696 (1993).

73. Vaia, R. A., Vasudevan, S., Krawiec, W., Scanlon, L. G. & Giannelis, E. P. New polymer electrolyte nanocomposites: Melt intercalation of poly (ethylene oxide) in mica-type silicates. *Adv. Mater.* **7,** 154–156 (1995).

74. Powell, C. E. Preparation of rubber compositions with organoclays. (2005). at <https://www.google.com/patents/CA2486039A1?cl=en>

75. Kato, M. & Usuki, A. in *Polymer-Clay Nanocomposites* (eds. Pinnavaia, T. J. & Beall, G. W.) (John Wiley & Sons, Inc., 2000).

76. Beall, G. W. & Powell, C. E. *Fundamentals of Polymer-Clay Nanocomposites.* (Cambridge University Press, 2011). at <https://books.google.at/books?id=-hohBWctFpgC>

77. Buchmaier, C. Synthese und Charakterisierung von lumineszierenden Zinksulfid-Polymer Nanokompositen. (Graz University of Technology, 2012).

78. Lange, L. & Triebel, W. in *Ullmann's Encyclopedia of Industrial Chemistry* (Wiley-VCH Verlag GmbH & Co. KGaA, 2000). doi:10.1002/14356007.a25_443

79. Wu, D. *et al.* Design and preparation of porous polymers. *Chem. Rev.* **112,** 3959–4015 (2012).

80. Yordanov, N. D., Gancheva, V., Mladenova, B. & Grampp, G. Kinetic studies on the reaction between copper(II) ions and some dithiocarbonates using stopped-flow technique. *Inorg. Chem. Commun.* **6,** 54–57 (2003).

81. Marsh, H. & Reinoso, F. R. *Activated Carbon.* (Elsevier Science, 2006). at <https://books.google.at/books?id=UaOXSk2vFVQC>

82. Mydriatic. No Title. at <http://upload.wikimedia.org/wikipedia/commons/6/65/Activated_Charcoal.jpg>

83. Sigma-Aldrich Co. LLC. S6760 Sigma. at <http://www.sigmaaldrich.com/catalog/product/sigma/s6760?lang=de&region=AT>

84. Wang, Z. & Fingas, M. Analysis of sorbitan ester surfactants. Part I: Capillary supercritical fluid chromatography. *J. High Resolut. Chromatogr.* **17,** 15–19 (1994).

85. Wang, Z. & Fingas, M. Analysis of sorbitan ester surfactants. Part II: Capillary supercritical fluid chromatography. *J. High Resolut. Chromatogr.* **17,** 85–90 (1994).

86. Rath, T. *et al.* A direct route towards polymer/copper indium sulfide nanocomposite solar cells. *Adv. Energy Mater.* **1,** 1046–1050 (2011).

87. FIZ Karlsruhe – Leibniz-Institut für Informationsinfrastruktur. ICSD.

88. Dutrow, B. L. & Clark, C. M. X-ray Powder Diffraction (XRD). at <http://serc.carleton.edu/18400>

89. Zhao, P., Huang, T. & Huang, K. Fabrication of indium sulfide hollow spheres and their conversion to indium oxide hollow spheres consisting of multipore nanoflakes. *J. Phys. Chem. C* **111,** 12890–12897 (2007).

90. Kaltenhauser, V. In situ synthesis of metal sulphide / polymer nanocomposites in single junction and tandem solar cells. (Graz University of Technology, 2013).